

# JOINT TRANSPORTATION RESEARCH PROGRAM

INDIANA DEPARTMENT OF TRANSPORTATION  
AND PURDUE UNIVERSITY



## Verification of Bridge Foundation Design Assumptions and Calculations



**Fei Han, Monica Prezzi, Rodrigo Salgado,  
Mehdi Marashi, Timothy Wells, Mir Zaheer**

## RECOMMENDED CITATION

Han, F., Prezzi, M., Salgado, R., Marashi, M., Wells, T., & Zaheer, M. (2020). *Verification of bridge foundation design assumptions and calculations* (Joint Transportation Research Program Publication No. FHWA/IN/JTRP-2020/18). West Lafayette, IN: Purdue University. <https://doi.org/10.5703/1288284317084>

## AUTHORS

### **Fei Han**

Postdoctoral Associate  
Lyles School of Civil Engineering  
Purdue University

### **Monica Prezzi, PhD**

Professor of Civil Engineering  
Lyles School of Civil Engineering  
Purdue University

### **Rodrigo Salgado, PhD**

Charles Pankow Professor of Civil Engineering  
Lyles School of Civil Engineering  
Purdue University  
(765) 494-5030  
[rodrigo@ecn.purdue.edu](mailto:rodrigo@ecn.purdue.edu)  
*Corresponding Author*

### **Mehdi Marashi**

Graduate Research Assistant  
Lyles School of Civil Engineering  
Purdue University

### **Timothy Wells, PE**

Research Section Manager  
Indiana Department of Transportation

### **Mir Zaheer, PE**

Geotechnical Design Engineer  
Indiana Department of Transportation

## ACKNOWLEDGEMENTS

The work presented in this report was funded by the Joint Transportation Research Program (JTRP) administered by the Indiana Department of Transportation (INDOT) and Purdue University through contract SPR-4165. The support of the Indiana Department of Transportation (INDOT) and the Federal Highway Administration (FHWA) are gratefully acknowledged. The continuous support received from the JTRP director, Darcy Bullock, the director of INDOT Research and Development, Barry Partridge, and the Chief Engineer of INDOT, Jeremy Hunter is greatly appreciated. The assistance of the JTRP staff and, in particular, the support received from the Study Advisory Committee members (Athar Khan, Peter Becker, Mahmoud Hailat, Youlanda Belew, and Matthew Kohut) is much appreciated. We greatly appreciate the assistance provided by the INDOT staff (Michael Brinkerhoff, Ben Crone, Debbie Calder, Jonathan Paauwe, and Erik Seef), the Superior Construction Company, Inc. staff (Jeff Carlson and Patric Tuuk), and Parsons Corporation engineers (Sean Porter and Derek Barnes). The authors thank Eshan Ganju, Nathan Bar, Abhishek Sakleshpur, Qian Hu, and Juliana Pereira for their help in instrumentation and measurements.

## JOINT TRANSPORTATION RESEARCH PROGRAM

The Joint Transportation Research Program serves as a vehicle for INDOT collaboration with higher education institutions and industry in Indiana to facilitate innovation that results in continuous improvement in the planning, design, construction, operation, management and economic efficiency of the Indiana transportation infrastructure. [https://engineering.purdue.edu/JTRP/index\\_html](https://engineering.purdue.edu/JTRP/index_html)

Published reports of the Joint Transportation Research Program are available at <http://docs.lib.purdue.edu/jtrp/>.

## NOTICE

The contents of this report reflect the views of the authors, who are responsible for the facts and the accuracy of the data presented herein. The contents do not necessarily reflect the official views and policies of the Indiana Department of Transportation or the Federal Highway Administration. The report does not constitute a standard, specification or regulation.

# TECHNICAL REPORT DOCUMENTATION PAGE

<b>1. Report No.</b> FHWA/IN/JTRP-2020/18	<b>2. Government Accession No.</b>	<b>3. Recipient's Catalog No.</b>	
<b>4. Title and Subtitle</b> Verification of Bridge Foundation Design Assumptions and Calculations		<b>5. Report Date</b> July 2020	
		<b>6. Performing Organization Code</b>	
<b>7. Author(s)</b> Fei Han, Monica Prezzi, Rodrigo Salgado, Mehdi Marashi, Timothy Wells, and Mir Zaheer		<b>8. Performing Organization Report No.</b> FHWA/IN/JTRP-2020/18	
<b>9. Performing Organization Name and Address</b> Joint Transportation Research Program (SPR) Hall for Discovery and Learning Research (DLR), Suite 204 207 S. Martin Jischke Drive West Lafayette, IN 47907		<b>10. Work Unit No.</b>	
		<b>11. Contract or Grant No.</b> SPR-4165	
<b>12. Sponsoring Agency Name and Address</b> Indiana Department of Transportation State Office Building 100 North Senate Avenue Indianapolis, IN 46204		<b>13. Type of Report and Period Covered</b> Final Report	
		<b>14. Sponsoring Agency Code</b>	
<b>15. Supplementary Notes</b> Conducted in cooperation with the U.S. Department of Transportation, Federal Highway Administration.			
<b>16. Abstract</b> <p>The Sagamore Parkway Bridge consists of twin parallel bridges over the Wabash River in Lafayette, IN. The old steel-truss eastbound bridge was demolished in November 2016 and replaced by a new seven-span concrete bridge. The new bridge consists of two end-bents (bent 1 and bent 8) and six interior piers (pier 2 to pier 7) that are founded on closed-ended and open-ended driven pipe piles, respectively. During bridge construction, one of the bridge piers (pier 7) and its foundation elements were selected for instrumentation for monitoring the long-term response of the bridge to dead and live loads. The main goals of the project were (1) to compare the design bridge loads (dead and live loads) with the actual measured loads and (2) to study the transfer of the superstructure loads to the foundation and the load distribution among the piles in the group. This report presents in detail the site investigation data, the instrumentation schemes used for load and settlement measurements, and the response of the bridge pier and its foundation to dead and live loads at different stages during and after bridge construction. The measurement results include the load-settlement curves of the bridge pier and the piles supporting it, the load transferred from the bridge pier to its foundation, the bearing capacity of the pile cap, the load eccentricity, and the distribution of loads within the pier's cross section and among the individual piles in the group. The measured dead and live loads are compared with those estimated in bridge design.</p>			
<b>17. Key Words</b> bridge monitoring, open-ended pipe piles, dead load, live load, pile group, pile cap, bridge design		<b>18. Distribution Statement</b> No restrictions. This document is available through the National Technical Information Service, Springfield, VA 22161.	
<b>19. Security Classif. (of this report)</b> Unclassified	<b>20. Security Classif. (of this page)</b> Unclassified	<b>21. No. of Pages</b> 33	<b>22. Price</b>

## EXECUTIVE SUMMARY

### Introduction

The Sagamore Parkway Bridge consists of twin parallel bridges over the Wabash River in Lafayette, IN. The old steel-truss eastbound bridge was demolished in November 2016 and replaced by a new seven-span concrete bridge. The new bridge consists of two end-bents (bent 1 and bent 8) and six interior piers (pier 2 to pier 7) that are founded on closed-ended and open-ended driven pipe piles, respectively. During bridge construction, one of the bridge piers (pier 7) and its foundation elements were instrumented with sensors to monitor the bridge response to dead and live loads. The main goals of the project were (1) to compare the design bridge loads (dead and live loads) with the actual measured loads and (2) to study the transfer of the superstructure loads to the foundation and the distribution of loads among the piles in the group.

This report presents, in detail, the site investigation data, the instrumentation schemes used for load and settlement measurements, and the response of the bridge pier and its foundation to dead and live loads at different stages during and after bridge construction. The measurement results include the load-settlement curves of the bridge pier and the piles supporting it, the load transferred from the bridge pier to the foundation elements, the bearing capacity of the pile cap, the load eccentricity, and the distribution of loads within the pier's cross section and among the individual piles in the group. The measured dead and live loads are compared with those estimated in bridge design.

### Findings

The load-settlement response of pier 7 under the dead loads during the construction of the bridge was almost linear. Pier 7 settled by 2.7 mm from the completion of the construction of the hammer head on January 18, 2018, to March 17, 2020. The pile head settlement from pile installation on November 15, 2016, to March 17, 2020, was estimated to be 5.2 mm. The secant stiffness of an average pile in the 3×5 pile group supporting pier 7 calculated at a settlement level of 5 mm was 46.4 kips/mm—this is about 61% (76.4 kips/mm) of the single, isolated test pile, as obtained from the static pile load test performed in 2016. At the end of the bridge construction on November 16, 2018, the piles under pier 7 carried about 77% (= 3,725 kips) of the total dead load (= 4,869 kips applied on the pile cap; it includes the weight of the bridge deck, beams, pier, pile cap, and back fill), while the remaining 23% (1,145 kips) was carried by the pile cap resting on soil. The average dead load per pile supporting pier 7 was measured to be 248 kips at the completion of the bridge construction. Assuming that the dead load carried by the soil under the pile cap was zero (to be consistent with the assumption made during bridge design) and that all the dead load was carried by the piles, the average dead load per pile would be 325 kips, which is in close agreement with the unfactored design dead load of 336 kips per pile.

A live load test was performed in March 2019 by parking twelve loaded triaxle trucks at specified locations on the bridge deck near pier 7. The live loads (resulting from the truck loads) measured in the bridge pier and on the pile heads increased as the trucks approached the pier and decreased to nearly zero as the trucks left the bridge. The eccentricity (of 5 ft) of the live loads (due to the asymmetric driveway lane design) resulted in uneven load distribution in the bridge pier and among the fifteen piles in the

group supporting it. The maximum live load (at step 4) in the pier was 460 kips (2,046 kN), corresponding to a ratio of 16% between the live load and the dead load in the bridge pier loaded with twelve loaded triaxle trucks. About half of the live load applied on the bridge pier was carried by the piles, while the remaining half of the live load was carried by the soil below the pile cap. In contrast, about 77% of the dead load was carried by the piles at the end of the bridge construction. The maximum vertical live load carried by a pile in the group under pier 7 was measured as 23 kips during the live load test. Assuming that the load carried by the pile cap was fully transferred to the piles, the maximum live load carried by a pile in the group supporting pier 7 is 53 kips. This is in close agreement with the maximum unfactored live loads in a pile obtained from simulations performed by Parsons Corporation on the live load test; the maximum unfactored live loads in a pile are 62 kips and 51 kips assuming continuous-span and simple-span bridge models, respectively.

### Implementation

Several implementation items were identified from this research project: (1) a developed instrument scheme that can be applied in other bridge projects, (2) suggestions on how to consider pile cap capacity and pile group effects in projects similar to the Sagamore Parkway Bridge project, (3) a validated design method for open-ended pipe piles, and (4) the continuous wireless monitoring of the foundations of the Sagamore Parkway Bridge.

A unique instrumentation scheme (as detailed in Chapter 3) was developed in this project for the short- and long-term monitoring of the performance of bridges subjected to dead and live loads. Using the developed instrumentation schemes, it was possible to measure the bridge pier settlement with submillimeter accuracy, even in the absence of access to the bridge pier (as when the site is flooded or when there are piers located in the river) and to monitor the load transfer from the superstructure to the foundation elements, both during construction and under service conditions. With the detailed instrumentation steps provided in this report, the instrumentation schemes followed for the Sagamore Parkway Bridge can be easily implemented in similar bridge projects to monitor the response of pile foundations to loads. Monitoring of the performance of bridge foundations is highly recommended whenever deemed feasible by INDOT: instrumentation cost is low compared with the cost of bridge design and construction, and the data from load and settlement measurements is of significant value. The high-quality monitoring data not only lays the basis for the improvement of foundation design methods and bridge design, but also enables the evaluation of the performance of bridges in a quantitative manner.

The contribution of the pile cap to the bearing capacity of the foundation of pier 7 was monitored for a period of almost 3 years. The pile cap resistance, which is the resistance carried by the soil under the pile cap, is typically ignored in routine bridge design. It was measured to be at least 20% of the dead load and about 50% of the live load. This means that the pile cap resistance could be considered in foundation design at least for piers that are not prone to scour (e.g., piers that are located on the riverbank or those located below the scour depth), leading to significant time and cost savings for INDOT. The cap resistance is dependent on a number of factors, including the size of the pile cap, pile group layout, and the soil profile below the pile cap. The ratio of the cap resistance to the total foundation resistance obtained in this research is only applicable to similar foundation layouts and soil conditions. Further research is needed to study the contribution of the pile cap to the overall bearing capacity of foundation under a wide range of scenarios.



According to the measurements made in this project, the response of an average pile in a pile group to axial loads is different from that of a single pile due to the pile-soil-pile interaction. The load-settlement stiffness of an average pile in the group is smaller (by about 40% for the present case) than that of a single pile in the same soil profile. This is consistent with the findings obtained from advanced numerical simulations for a pile group of similar size and configuration as that of pier 7. The different load-settlement stiffnesses of a single pile and an average pile in a group should be considered in bridge foundation design, especially for cases in which the vertical settlement is critical in design.

The monitoring of the bridge pier over the course of this project shows that the bridge has performed very well under dead and live loads, proving the successful foundation design based on the high-quality data obtained from the static load tests performed at the site. An example of the design of a production pile that follows the LRFD framework and uses the data obtained from the static pile load test is provided in this report as reference for future bridge foundation designs by INDOT. The dead loads measured during bridge construction agree closely with those estimated in the bridge design. Furthermore, the maximum live load measured during the live load test is in close agreement with the live loads obtained from simulations of the live load test done by Parsons Corporation for a continuous-span bridge and a simple-span bridge.

Continuous monitoring of the Sagamore Parkway Bridge using a wireless data acquisition (DAQ) system is strongly recommended to continue to study the long-term performance of the bridge under service since all the sensors are fully functional; this is due to the careful instrumentation procedures followed and the effective protection of the sensors and cables from damage during concrete pouring. With the continuous monitoring of the bridge pier and foundation, we will be able to study the effects water table fluctuation, potential scour during extreme weather events, and dynamic loads due to traffic and wind have on long-term bridge performance. This would be a valuable addition to this unique case history considering the completeness of the dataset, which included full site investigation and soil characterization, dynamic and static load tests on fully instrumented test piles, load and settlement monitoring of the bridge pier and its foundation elements under dead and live loads during and after bridge construction. With the implementation of a wireless DAQ system, engineers and researchers will be able to monitor the bridge performance from their office in real time. This is expected to significantly improve the efficiency of data collection (by eliminating or reducing the need for frequent site visits) and to ensure the safety of transportation infrastructure. Instrumentation schemes similar to the ones used in this project can be implemented at other bridge sites to augment the dataset acquired in this project and improve the design and performance of bridge and foundations in the state of Indiana.

## CONTENTS

1. INTRODUCTION . . . . .	1
1.1 Background . . . . .	1
1.2 Project Overview . . . . .	1
1.3 Report Structure . . . . .	2
2. SITE INVESTIGATION . . . . .	2
2.1 Topography and Geology . . . . .	2
2.2 In Situ Tests . . . . .	2
3. INSTRUMENTATION OF THE BRIDGE PIER AND FOUNDATION . . . . .	5
3.1 Settlement Measurements . . . . .	5
3.2 Load Measurements . . . . .	6
4. MEASUREMENT OF THE DEAD LOADS FROM THE BRIDGE . . . . .	9
4.1 Construction Stages . . . . .	9
4.2 Load-Settlement Curve . . . . .	11
4.3 Load Transfer from the Superstructure to the Foundation . . . . .	12
4.4 Distribution of the Dead Loads Among Piles in the Group . . . . .	14
5. LIVE LOAD TEST . . . . .	15
5.1 Test Procedure . . . . .	15
5.2 Test Results . . . . .	17
6. DESIGN OF BRIDGE FOUNDATIONS . . . . .	19
6.1 Comparison Between the Design Loads and Measured Loads . . . . .	19
6.2 LRFD Design of the Bridge Foundations . . . . .	21
7. SUMMARY AND CONCLUSION . . . . .	23
REFERENCES . . . . .	23

## LIST OF TABLES

Table	Page
<b>Table 2.1</b> Soil profile near pier 7	5
<b>Table 3.1</b> Gauge factors for the sensors used in the bridge pier and on the pile heads	8
<b>Table 4.1</b> Construction stages of pier 7 of the Sagamore Parkway Bridge over Wabash River	10
<b>Table 4.2</b> The settlement criteria for bridge piers and foundations in the literature	12
<b>Table 5.1</b> The weight (in kips) of the twelve trucks used for the live load test	15
<b>Table 5.2</b> The numbers of trucks positioned at the specified locations on the bridge deck in each load step during the live load test	16
<b>Table 6.1</b> Maximum live loads for pier 7 and for the piles supporting it, according to different approaches	20
<b>Table 6.2</b> Unit shaft resistance $q_{sL}$ obtained from the static load test on the open-ended pipe pile	22
<b>Table 6.3</b> Dimensions used to calculate the bearing capacity of the piles supporting pier 7	22
<b>Table 6.4</b> LRFD design check for production piles at pier 7	22

## LIST OF FIGURES

Figure	Page
<b>Figure 1.1</b> Side view of the seven-span Sagamore Parkway eastbound bridge over the Wabash River, the span lengths between piers, and the dead loads at the bottom of each pier	1
<b>Figure 2.1</b> Surface geology and physiographic divisions of Indiana	3
<b>Figure 2.2</b> Locations of the SPTs and CPTs performed at the test site	3
<b>Figure 2.3</b> In situ test results versus depth: SPT blow counts ( $N_{SPT}$ ), CPT cone resistances ( $q_c$ ), mean particle size ( $D_{50}$ ), and gravel content. The ground elevation is at 522 ft in the figure	4
<b>Figure 2.4</b> Grain size distribution of the soils collected at various depths: (a) from 15 to 40 ft, (b) from 45 to 65 ft, (c) from 70 to 90 ft, and (d) from 95 to 110 ft	4
<b>Figure 3.1</b> Scheme for settlement measurement: (a) locations of pier 7 of the eastbound bridge, the reference station, and the old pier of the westbound bridge, (b) the barcode sticker attached to pier 7 and the old pier of the westbound bridge, and (c) the position of the digital level with respect to the reference station and the bridge pier	6
<b>Figure 3.2</b> Strain gauges installed in the cross section of the pier and the tributary area associated with each sensor	7
<b>Figure 3.3</b> Installation of sensors in the bridge pier: (a) installation of the rebar (sister-bar) strain gauge and (b) installation of the concrete-embedded strain gauge	7
<b>Figure 3.4</b> Installation of the arch-weldable VW strain gauges on the pile head: (a) components of the strain gauge and (b) protection of the strain gauge	8
<b>Figure 3.5</b> Strain gauge cable arrangement and protection: (a) arrangement of the gauge cables along the reinforcement rebars in the pile cap and (b) protection of the gauge cables using polyethylene foam	9
<b>Figure 3.6</b> The structural and foundation components of pier 7, the locations of the sensors installed in the bridge pier and on the foundation elements, and the arrangement of the sensor cables	9
<b>Figure 4.1</b> Total load applied on the pile cap versus the corresponding settlement of pier 7 measured at different stages during and after bridge construction	10
<b>Figure 4.2</b> The load-settlement curve of the test pile obtained from the pile load test performed in 2016 and that of an average production pile in the $3 \times 5$ pile group under pier 7 of the Sagamore Parkway Bridge over the Wabash river	11
<b>Figure 4.3</b> The load-settlement curves of a single pile and an average pile in a $4 \times 4$ pile group in dense sand ( $D_R = 80\%$ )	12
<b>Figure 4.4</b> Total load applied on the pile cap and total load carried by the piles in the group measured at different stages during and after the bridge construction	13
<b>Figure 4.5</b> Contribution of the pile cap to the bearing capacity of the pile group: (a) the equilibrium of forces applied on the pile cap and (b) the $Q_{pg}/Q_{total}$ and $Q_{cap}/Q_{total}$ ratios obtained at different stages	13
<b>Figure 4.6</b> Layout of the pile group and cross section of the pile cap under pier 7	14
<b>Figure 4.7</b> Distribution of dead loads among piles in the group at different stages during and after bridge construction	14
<b>Figure 5.1</b> Locations on the bridge deck where the live loads were applied (the configuration for load step 4 is shown in the figure)	15
<b>Figure 5.2</b> Live load test in progress: (a) settlement measurement for pier 7 and (b) loaded trucks on the bridge deck applying the live loads	16
<b>Figure 5.3</b> Live loads applied on the bridge: (a) top view of the bridge deck with the trucks that were used to apply the live loads and (b) cross section of the bridge at pier 7 and the eccentricity of the resultant live load	16
<b>Figure 5.4</b> Live load distribution over the cross section of the bridge pier at each load step during the live load test	17
<b>Figure 5.5</b> Calculation of the eccentricity $e$ of the resultant live load. The distance $d_i$ is positive above the neutral axis and negative below the neutral axis	17
<b>Figure 5.6</b> Distribution of the live loads at the heads of the fifteen piles in the group at different load steps during the live load test	18
<b>Figure 5.7</b> Load-settlement curve: (a) for the bridge pier and (b) for an average pile in the group	19
<b>Figure 5.8</b> The live load in the bridge pier (pier 7) versus the total load carried by all the piles during the live load test	19
<b>Figure 6.1</b> Static pile load test performed on instrumented open-ended test pile at the Sagamore Parkway Bridge site	21

## 1. INTRODUCTION

### 1.1 Background

In bridge design, assumptions are made to estimate the dead and live loads when designing both the superstructure and the foundation elements (AASHTO, 2018). There is considerable reliance on values of loads prescribed in codes (AASHTO, 2018; INDOT, 2013). Ideally, design assumptions would be verified after bridge construction to allow for improvement in design codes and assumptions over time; however, this is rarely done.

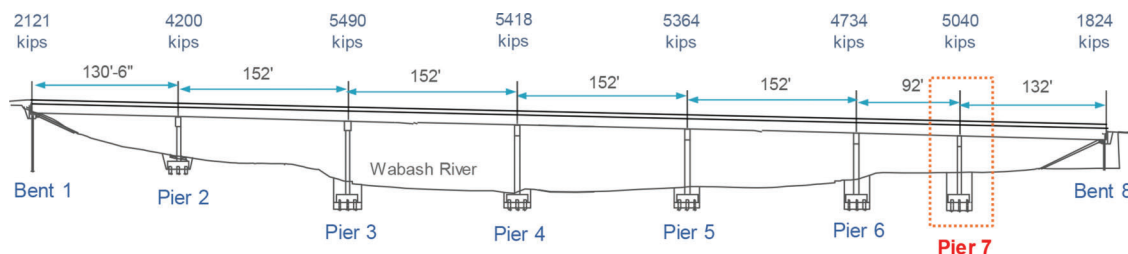
A database consisting of high-quality measurements of the actual loads carried by the structural and foundation elements of different types of bridges would be very helpful in reducing the degree of conservatism in design, leading to more cost-effective designs while maintaining the safety and serviceability of bridges. However, only a limited number of studies have been performed for this purpose. Dasenbrock, Mattison, and Budge (2012) studied the effect of live loads on the pile foundation of the abutment of a two-span bridge. In their study, two of the sixteen piles were instrumented with vibrating-wire strain gauges along the pile length to measure the load transfer upon live load application. Mandolini, Russo, and Viggiani (2005) reported a case history on the load measurements made for a piled raft supporting the main pier of a cable-stayed bridge (the Garigliano Bridge in southern Italy) during and after construction. They installed load cells on 35 piles, out of the 144 piles supporting the pier, and 8 pressure cells between the raft and the soil below it in order to measure the load distribution between the piles and the raft. Similar studies have been reported in which the load carrying capacity of foundation elements supporting high-rise buildings was measured. Shulyat'ev and Kharichkin (2009) measured the load distribution among six representative piles, instrumented with strain gauges on the pile heads, of a large pile group supporting a high-rise building. Yamashita, Yamada, and Hamada (2011) studied the load sharing between the piles and the rafts of seven high-rise buildings supported on pile rafts during and after completion of construction (one to two piles were instrumented in each case). More case studies like the ones reported herein are needed to develop the understanding of the response of bridge foundations subjected to dead and live loads during and after construction and to verify

and improve the assumptions made in the design of bridge foundations.

### 1.2 Project Overview

The Sagamore Parkway Bridge consists of twin, parallel bridges over the Wabash River in Lafayette, IN (40°27'05.7"N 86°53'39.3"W). The old steel-truss eastbound bridge was demolished in November 2016 and replaced by a new seven-span concrete bridge (as shown in Figure 1.1) designed by Parsons Consulting Engineers and constructed by Superior Construction in a period of about 2 years. The new eastbound bridge is founded on two end-bents (bent 1 and bent 8) and six interior piers (pier 2 to pier 7). During construction, the research team from Purdue University had a unique opportunity to instrument one of the bridge piers (pier 7) and its foundation elements with sensors to monitor the long-term response of the bridge pier under dead and live loads.

In this report, we present the results of the site investigation, the detailed instrumentation schemes used for load and settlement measurements, and the results of the measurements made at different stages during and after bridge construction of the bridge pier and its foundation elements subjected to dead and live loads. With the instrumentation of the bridge pier 7 and on all of the fifteen piles supporting it, the load transfer from the superstructure to the pier column, then to the pile cap, and to the individual piles in the group was monitored for about 3 years. When the superstructure load is applied on the pile cap, a portion of the load is carried by the soil below the pile cap (known as the cap resistance), and the remaining portion of the load is carried by the piles in the group. The load distribution between the pile cap and the piles in the group was investigated in this project to provide valuable insights for INDOT to consider accounting for the contribution of the pile cap in future foundation designs. The load-settlement response of all the fifteen production piles supporting pier 7 was obtained for dead and live loads. In order to understand pile-cap-soil interaction, the average load-settlement response of the production piles in the pile group supporting pier 7 was compared with that obtained from the static load test performed in 2016 on a fully-instrumented test pile at the same construction site. The load-settlement stiffness of an average pile in the group was smaller than that of the



**Figure 1.1** Side view of the seven-span Sagamore Parkway eastbound bridge over the Wabash River, the span lengths between piers, and the dead loads at the bottom of each pier.



single pile tested at the site. The measured dead and live loads were compared with those estimated for the design of the Sagamore Parkway Bridge to verify the assumptions usually made in bridge design. As an example, a production pile was designed following the LRFD framework and using the data obtained from the static pile load test.

### 1.3 Report Structure

Chapter 2 presents the geological features of the Sagamore Parkway Bridge site and the results of the site investigation carried out to characterize the soil profile at the site. The profiles of the CPT cone resistance  $q_c$  and SPT blow counts  $N_{SPT}$ , along with the basic properties of the soils in each soil layer of the profile (e.g., grain size distribution, particle morphologies, and gravel content) are reported in this chapter.

Chapter 3 details the instrumentation of the bridge pier (pier 7) and its foundation elements. The instrumentation allows for measurement of the pier settlement, the load transfer from the superstructure to the foundation elements, and the load distribution among the fifteen piles in the group supporting the bridge pier.

Chapter 4 and Chapter 5 report the measurement results of the response of the bridge subjected to dead and live loads, respectively. The results consist of the bridge pier settlement, the load transfer from the pier to the foundation elements, the load distribution among individual piles in the pile group supporting pier 7, the comparison of the load-settlement response of the production piles (in a  $3 \times 5$  group configuration) and that of a single pile tested in the context of project SPR-4040, and the load bearing capacity of the pile cap.

In Chapter 6, we compare the dead and live loads measured through bridge monitoring and those estimated in the bridge design. An LRFD design example is provided for a production pile using the data obtained from the static pile load test. Chapter 7 summarizes the main contents and findings presented in the report.

## 2. SITE INVESTIGATION

In order to obtain the soil stratigraphy at the test site, a series of Standard Penetration Tests (SPTs) and Cone Penetration Tests (CPTs) were performed in the area near pier 7. Soil samples were collected using the split-spoon sampler during the SPTs, and laboratory tests were performed on these soils to obtain their basic properties. The site investigation shows that the soil profile consists mainly of medium dense-to-dense, poorly-graded sand with varying gravel contents (Han, Ganju, Prezzi, et al., 2020; Han, Ganju, Salgado, & Prezzi, 2019).

### 2.1 Topography and Geology

The Wabash valley at the location of the Sagamore Parkway Bridge is about 1.5 miles wide and 200 ft deep

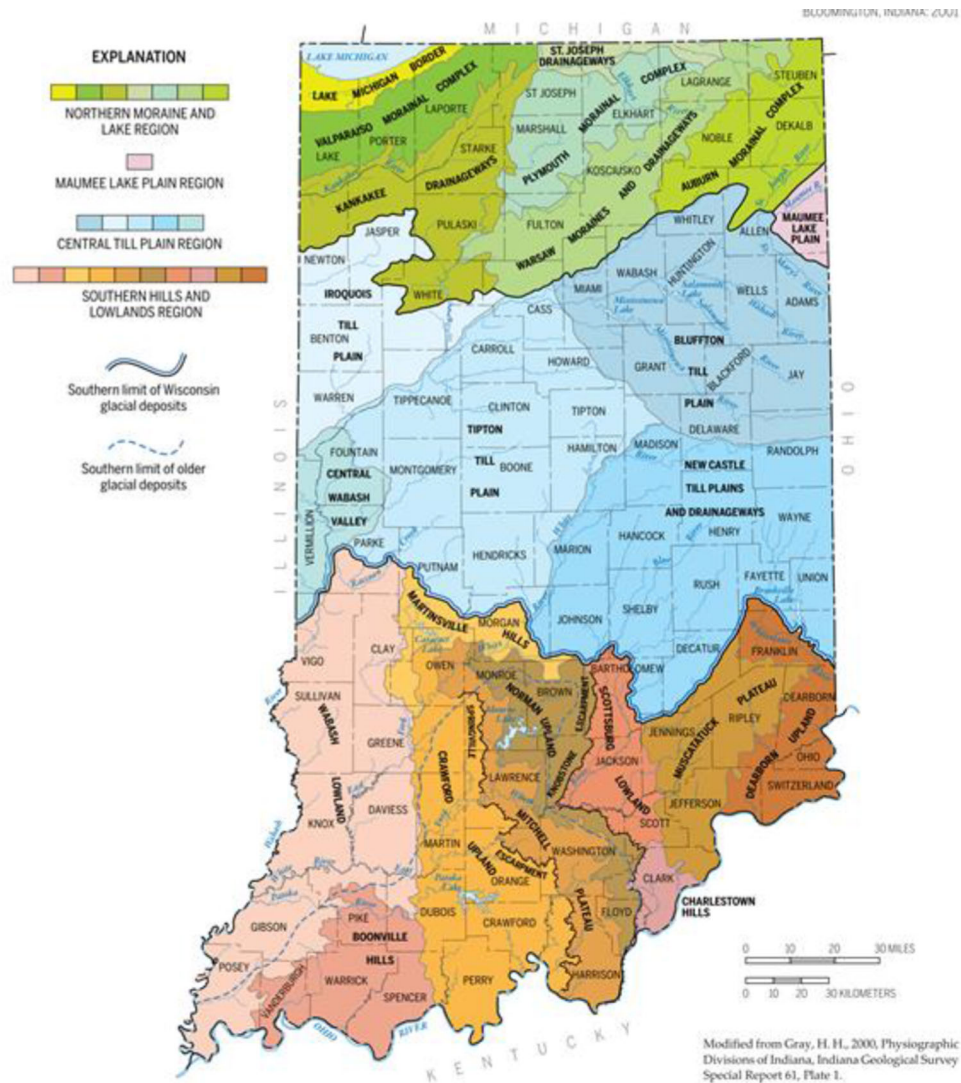
(Camp & Richardson, 1999). The elevation of the lowest point of the river cross-section along the bridge (the flowline) is at 500.94 ft above sea level, and the average river water level is at 510 ft above sea level. The slope of the western river bank is about 10%, whereas the eastern river bank has a slope of approximately 25% (Parsons, 2016).

Northern and central Indiana, where the test site is located at, is covered by Quaternary Wisconsin glacial deposits in the form of moraines in the north and till plains in central Indiana. The Wabash valley, for many miles upstream and downstream of the bridge, is part of the Tipton Till Plain, which is covered by 100 ft–200 ft of sand and gravel. These deposits typically consist of mixtures of sand and gravel. No bedrock outcrops are found near the location of the bridge (Camp & Richardson, 1999; West, 2000).

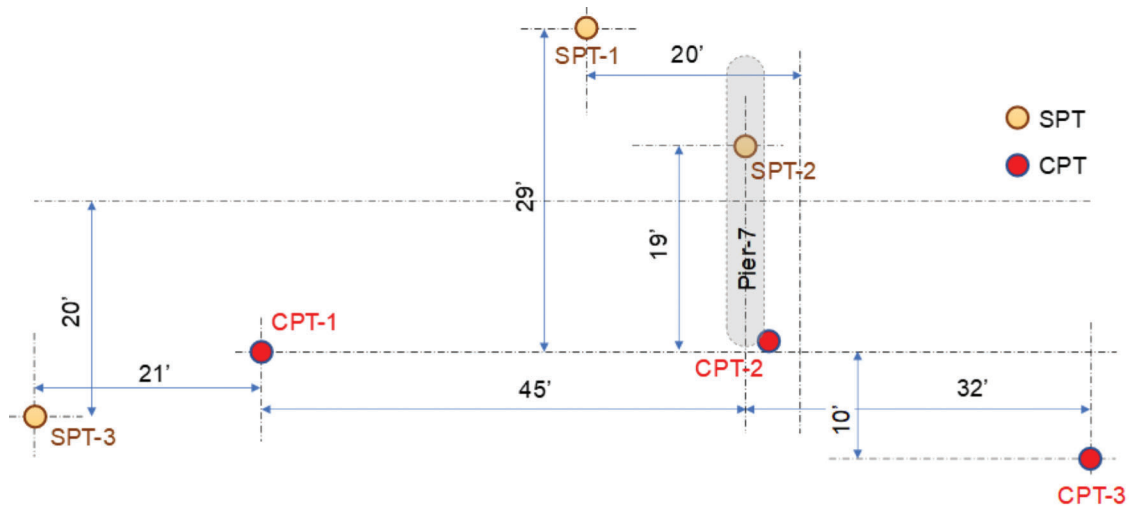
### 2.2 In Situ Tests

As shown in Figure 2.2, three SPT borings and three CPT soundings were performed at the test site within a 70-foot distance from pier 7 (Han, Ganju, Salgado, & Prezzi, 2019). The SPTs were performed at five-foot intervals, and none of the SPTs reached the bedrock. Figure 2.3 shows the profiles of the SPT blow counts and the CPT cone resistances obtained from these tests. Because of the high gravel content found in the soil profile, the cone penetration test reached refusal at about 60 ft below the ground surface. Since the bridge piles were expected to be longer than 100 ft, it was important to obtain the cone resistance  $q_c$  profile beyond this depth to be able to design the piles using CPT-based methods. Therefore, a unique drill-and-push scheme, as described by Han, Ganju, Prezzi, et al. (2020), that combines auger drilling and cone penetration was implemented in CPT-3 to obtain the cone resistance profile up to a depth of 107 ft. When the drilling through a gravel layer was completed and the cone penetration test was resumed, values of cone resistance over a length of three cone diameters ( $3 \times 44.6 = 134$  mm) below the base of the auger bit were discarded because of the possibility of soil disturbance within that zone during auger drilling.

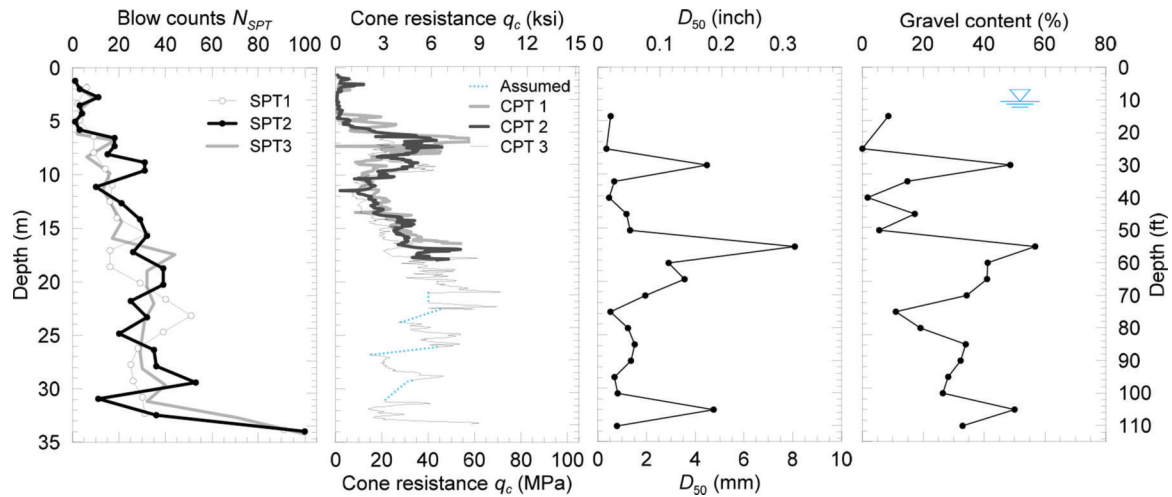
During the SPTs, a split-spoon driving sampler was used to collect soil samples from various depths. Laboratory tests, including sieve analyses and morphology tests, were performed on the soils collected from each layer to obtain their grain size distributions (as shown in Figure 2.4) and basic properties (as summarized in Table 2.1). Relatively low gravel content ( $<20\%$ ) was found above a depth of 50 ft, except in a single layer at a depth of 30 ft where high gravel content ( $>50\%$ ) was observed. The gravel content is generally in the range of 30%–50% below 50 ft, reaching as high as 60% at a depth of about 55 ft. Herein, any particle larger than 4.75 mm is considered gravel, as per the Unified Soil Classification System (ASTM D2487-17, 2017). Broken gravel pieces were observed in the



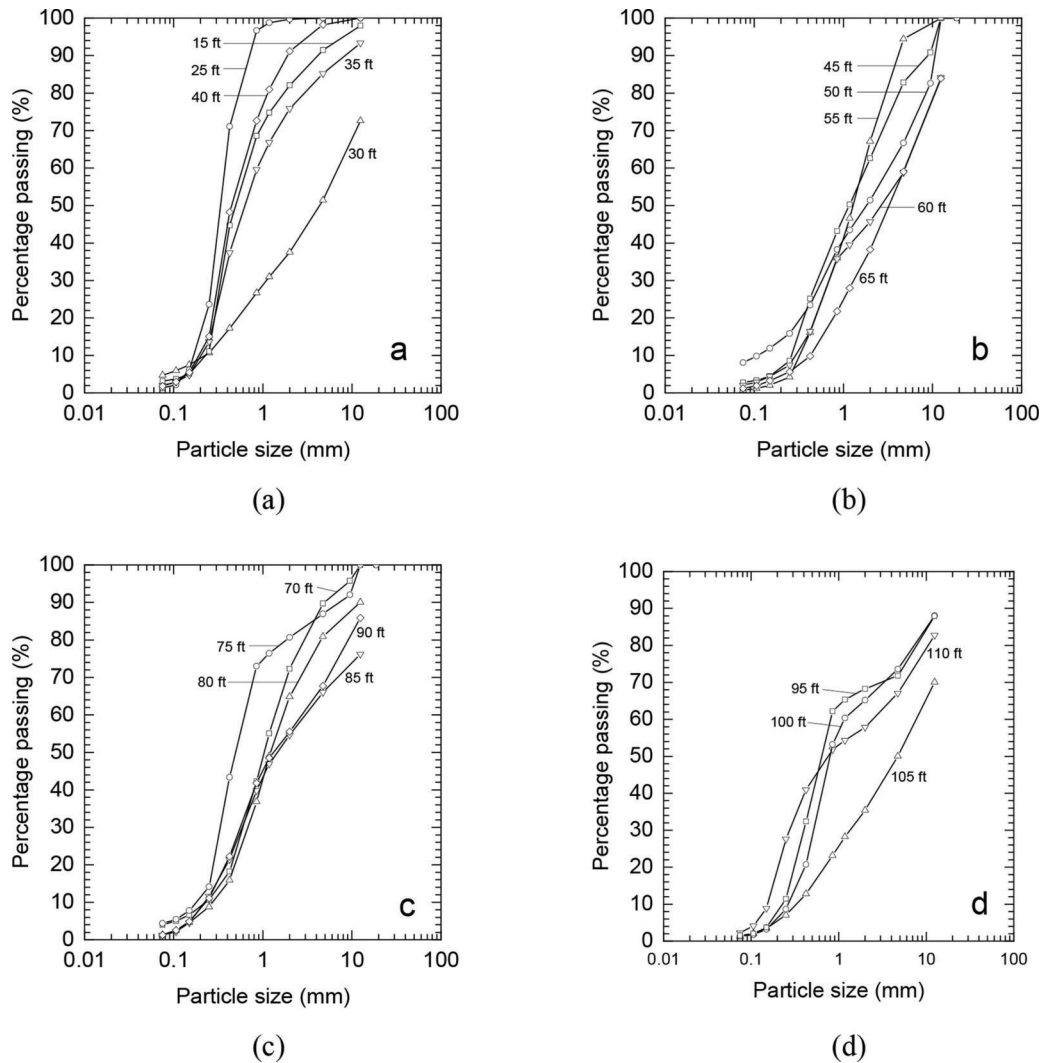
**Figure 2.1** Surface geology and physiographic divisions of Indiana (Gray, 2000, as cited in Hill, 2019).



**Figure 2.2** Locations of the SPTs and CPTs performed at the test site (modified after Han, Ganju, Salgado, & Prezzi, 2019).



**Figure 2.3** In situ test results versus depth: SPT blow counts ( $N_{SPT}$ ), CPT cone resistances ( $q_c$ ), mean particle size ( $D_{50}$ ), and gravel content. The ground elevation is at 522 ft in the figure (modified after Han, Ganju, Salgado, & Prezzi, 2019).



**Figure 2.4** Grain size distribution of the soils collected at various depths: (a) from 15 to 40 ft, (b) from 45 to 65 ft, (c) from 70 to 90 ft, and (d) from 95 to 110 ft (after Han, Ganju, Salgado, & Prezzi, 2019).

TABLE 2.1  
Soil profile near pier 7 (modified after Han, Ganju, Salgado, & Prezzi, 2019)

Layer No.	Depth (m)	Soil Description	$\gamma_t$ (kN/m <sup>3</sup> )	Gravel Content (%)	$D_{50}$ (mm)	$C_U$	$C_C$	R	S	USCS Classification
1	0–18	Clayey silt with sand	19.5	0	–	3.0	0.8	–	–	–
2	18–27	Sand with gravel	20.0	4	0.4	2.6	0.9	0.41	0.82	SP
3	27–34	Sandy gravel	21.5	49	4.5	34.6	0.7	0.44	0.82	SP
4	34–55	Sand with gravel	20.0	10	0.9	4.8	0.7	0.50	0.84	SP
5	55–74	Gravelly sand	21.5	43	4.1	16.6	0.6	0.46	0.81	SP
6	74–107	Gravelly sand	21.5	28	1.1	8.3	0.8	0.44	0.82	SP

Notes:

$\gamma_t$  = total unit weight

$D_{50}$  = mean particle diameter

$C_U$  = coefficient of uniformity =  $D_{60}/D_{10}$

$C_C$  = coefficient of curvature =  $(D_{30})^2/(D_{10} \times D_{60})$

R = roundness = the ratio of the average radius of curvature of the corners of the particle to the radius of the maximum circle that can be inscribed

S = sphericity = the ratio of the diameter of a circle with area equal to the projected area of the particle to the diameter of the circumscribing circle to the particle projected area

samples collected from the SPTs, suggesting the existence of larger particles in the soil profile that could not be collected by the SPT sampler, which has an inner diameter of 28.5 mm (Han, Ganju, Prezzi, et al., 2020).

### 3. INSTRUMENTATION OF THE BRIDGE PIER AND FOUNDATION

In order to measure the load transfer from the superstructure to the foundation elements and to obtain the load distribution among individual piles in the pile group subjected to dead and live loads, both the bridge pier and its foundation elements were instrumented with sensors. To take advantage of the extensive site investigation and the data that were obtained from the static pile load tests performed at the Sagamore Parkway Bridge site (Ganju et al., 2020; Han, Ganju, Prezzi, et al., 2020; Han, Ganju, Salgado, & Prezzi, 2019; Han, Ganju, Salgado, Prezzi, & Zaheer, 2019), pier 7 and its foundation elements were selected for instrumentation (pier 7 was the pier closest to the location of the static pile load tests previously performed in the context of the JTRP research project SPR 4040). The foundation for pier 7 consists of a 7-ft-thick pile cap resting on a group of fifteen (in a layout of 3 × 5) steel open-ended pipe piles. The instrumentation for settlement and load transfer measurements is detailed below.

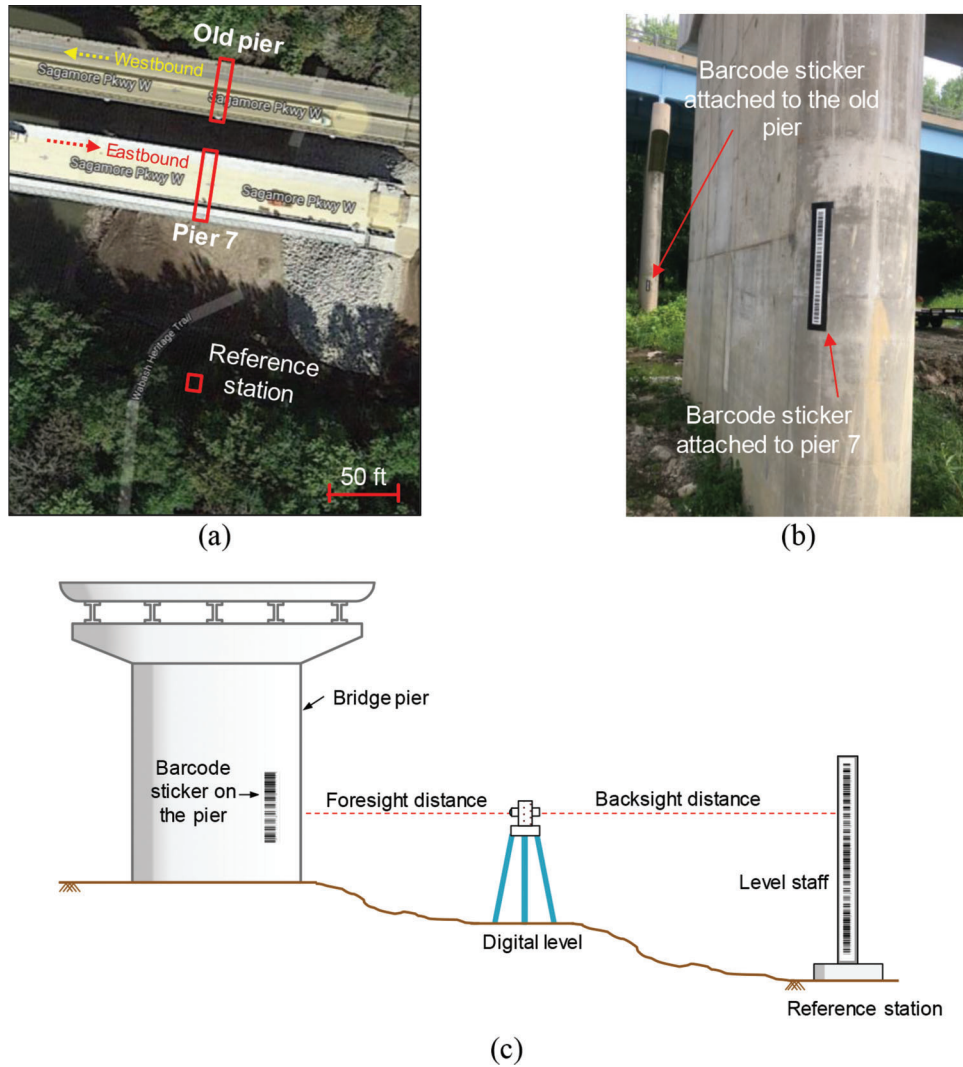
#### 3.1 Settlement Measurements

Traditional surveying techniques with a TOPCON DL-101C digital optical level were used to measure the settlement of the pier. The digital level uses a level staff with a barcode printed on it as its target (see Figure 3.1c). Using the barcode level staff and the digital level, elevations with submillimeter accuracy can be measured (TOPCON, 2011). In order to measure the

settlement of the bridge pier, it is necessary to have a stationary reference point on the ground. For that purpose, a reference station was built at a location outside the influence zone of the foundation and of construction activities on the site. A permanent concrete benchmark supported by four hand-driven steel micro-piles was constructed about 170 ft south of pier 7. In addition, the closest pier of the old westbound bridge to pier 7 was used as an auxiliary reference point (Figure 3.1a). This old pier was built on a pile group foundation about 50 years ago. The settlement of this old pier was measured periodically during the present study, and no settlement was observed, proving its feasibility as an auxiliary reference point.

In traditional elevation surveying (as illustrated in Figure 3.1c), the level is placed between the target object and the reference station; readings are taken from the level pointing at the level staff placed on top of the reference station and then on a fixed point on the target object. However, the ground near the bridge pier (pier 7) often becomes soft and inaccessible during the wet seasons, making it impossible to access the bridge pier for settlement measurements. To solve this problem, the barcode printed on the level staff was scanned using a high-resolution (600 dpi) flatbed scanner and printed 1:1 on laminated polymer stickers using a flatbed printer. The flatbed scanner scans the object being scanned by multiple passes with the scanning head maintained perpendicular to the object. To test the accuracy of this solution, trial elevation measurements were made using a dummy level staff with the barcode sticker attached to it and compared with measurements made using the standard level staff. The barcode sticker had the same level of accuracy (submillimeter) of the standard level staff. The barcode sticker was attached to the surface of pier 7 (as shown in Figure 3.1b) using a plumb bob and a level to ensure the verticality of the barcode sticker. Similarly, a barcode sticker was attached to the old pier of the





**Figure 3.1** Scheme for settlement measurement: (a) locations of pier 7 of the eastbound bridge, the reference station, and the old pier of the westbound bridge, (b) the barcode sticker attached to pier 7 and the old pier of the westbound bridge, and (c) the position of the digital level with respect to the reference station and the bridge pier.

westbound Sagamore Parkway Bridge for reference elevation readings. During each settlement measurement session, three sets of readings were taken, and the average settlement was reported to minimize any random errors. To minimize systematic errors, the digital level was regularly calibrated according to the instructions provided by the manufacturer. Additionally, the digital level was positioned at similar distances from the reference point and the bridge pier during each settlement measurement (Figure 3.1c).

### 3.2 Load Measurements

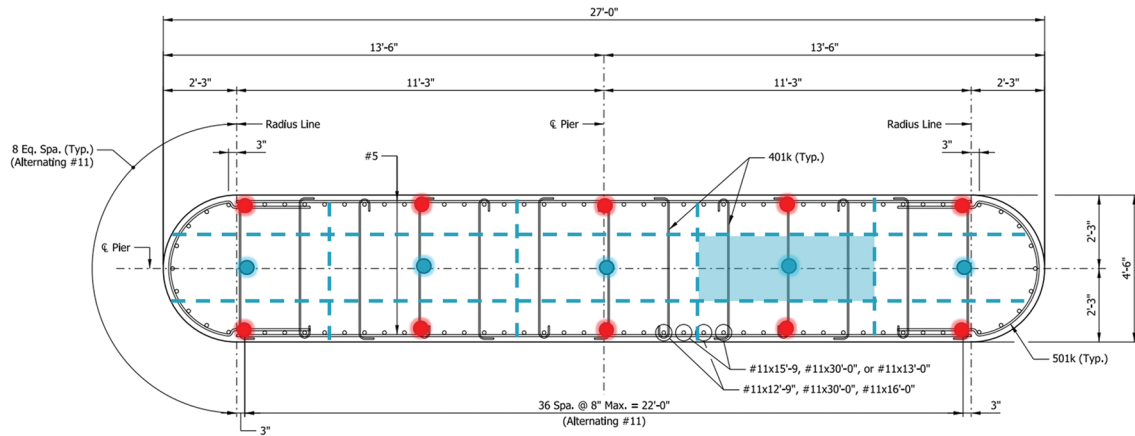
The loads applied to the bridge superstructure are transferred through the bridge pier to the foundation elements. To measure the loads carried by the bridge pier, ten rebar (sister-bar) vibrating-wire strain gauges (Geokon Model 4911) and five concrete-embedded vibrating-wire strain gauges (Geokon Model 4200) were

installed at a cross section 3 ft above the base of the bridge pier. The layouts of the sensors in this cross-section of the pier are shown in Figure 3.2. The rebar strain gauges were tied to the main vertical rebars using iron-tie wires (Figure 3.3a) along the perimeter of the bridge pier. The concrete-embedded strain gauges were fastened to the horizontal rebars using nylon cable ties (Figure 3.3b) along the neutral axis of the bridge pier.

To calculate the total axial load carried by the pier, the cross-section of the pier was divided into fifteen tributary areas, each one associated with one of the sensors (as shown in Figure 3.2). The total axial load  $Q_{\text{pier}}$  in the pier was calculated as the summation of the products of the strain  $\varepsilon_i$  measured from each sensor by the corresponding equivalent Young's modulus  $E_i$  and the tributary area  $A_i$ :

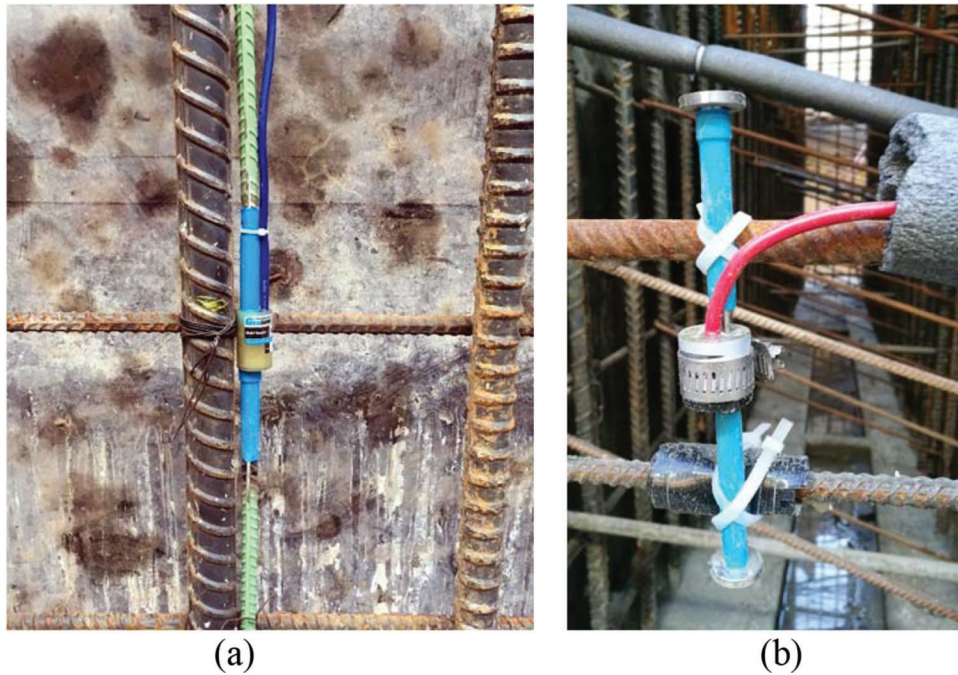
$$Q_{\text{pier}} = \sum E_i \varepsilon_i A_i \quad (\text{Equation 3.1})$$





- Rebar strain gauge
- Concrete embedded strain gauge
- Tributary area

**Figure 3.2** Strain gauges installed in the cross section of the pier and the tributary area associated with each sensor.



**Figure 3.3** Installation of sensors in the bridge pier: (a) installation of the rebar (sister-bar) strain gauge and (b) installation of the concrete-embedded strain gauge.

where the equivalent Young's modulus  $E_i$  is calculated as the area-weighted average of the Young's moduli  $E_c$  and  $E_s$  of the concrete and steel:

$$E_i = (E_s A_{Si} + E_c A_{Ci}) / A_i \quad (\text{Equation 3.2})$$

where  $A_{Ci}$  and  $A_{Si}$  are the areas of the concrete and steel in the  $i^{\text{th}}$  tributary area  $A_i$ . Four concrete samples were collected during pier pouring, and the collected samples were tested (ASTM C469/C469M, 2014) 42 days after

the pouring to obtain the Young's modulus  $E_c$  of the concrete ( $= 3,408$  ksi). The Young's modulus of the steel was assumed to be 29,000 ksi.

To measure the load distribution among the fifteen piles supporting pier 7, a pair of arc-weldable, vibrating-wire (VW) strain gauges (Geokon model 4000) were installed at the head of each pile. Each pair of strain gauges were welded on diametrically opposite sides (east and west sides) of the pile to cancel out any bending that might exist at the pile head. As shown in

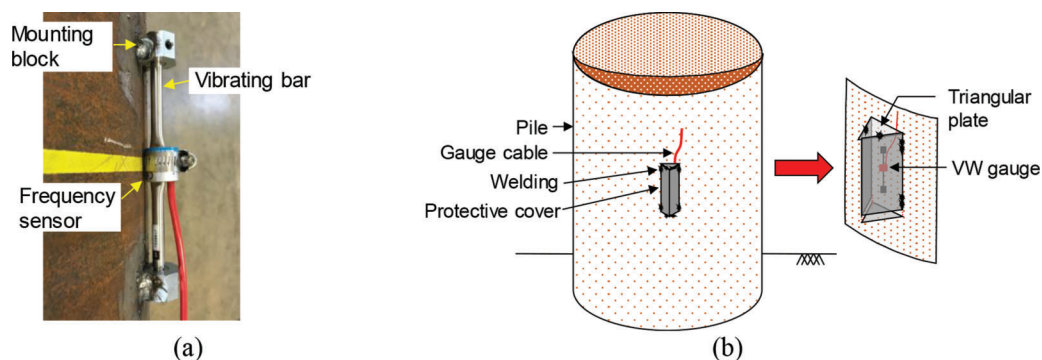
Figure 3.4, the installation of the VW strain gauges was carried out as follows:

1. Mark the location of the strain gauge on the pile surface.
2. Grind off any rust or debris on the pile surface at the location of the strain gauge using a hand-held grinder.
3. Position the two mounting blocks and weld them to the pile surface using a dummy vibrating bar.
4. Replace the dummy vibrating bar with the actual vibrating bar and frequency sensor (as shown in Figure 3.4a).

The load in each pile can be calculated by multiplying the average strain readings from the pair of sensors at the pile head by the axial stiffness ( $A_{pile} E_S$ ) of the pile. Table 3.1 summarizes the gauge factors used for all three types of strain gauges installed in the bridge pier and on the pile heads. All the sensors and their cables were carefully protected from damage during construction and long-term erosion. The arc-weldable strain gauges were covered using a protective steel angle welded over them on each side of the pile. To prevent fluid concrete from entering the steel angle during

concrete pouring, all openings on the steel angle were filled with the GREAT STUFF insulating foam sealant. The pile head sensor cables were systematically labeled and organized into two bundles (using zip ties) secured to the rebars of the pile cap (Figure 3.5a). The cable bundles were then wrapped in a protective polyethylene foam at 8-to-12-inch intervals (Figure 3.5b).

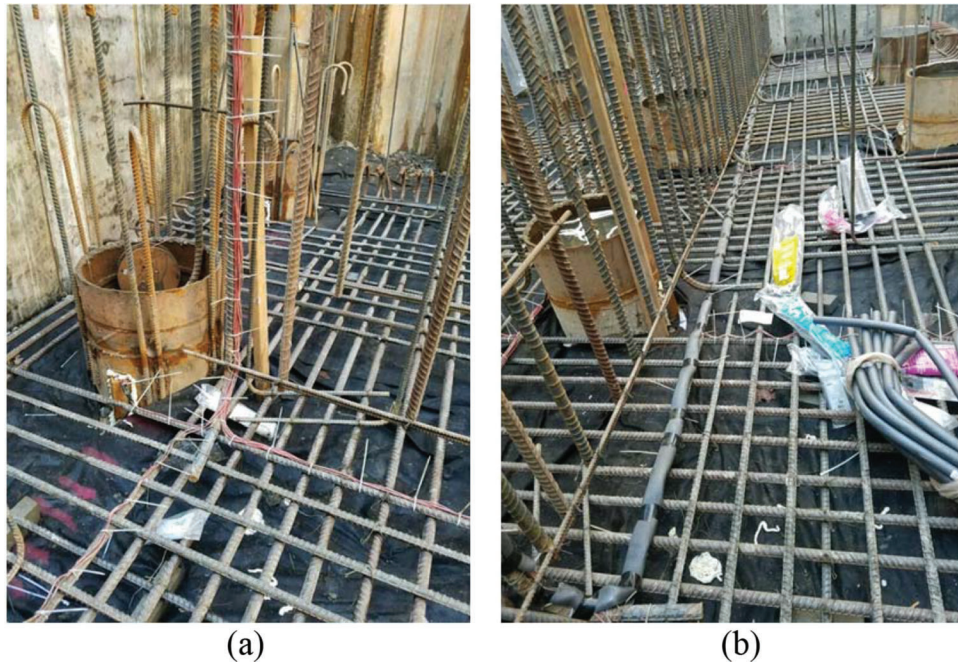
Figure 3.6 shows the locations of the sensors installed in the bridge pier and on the pile heads, as well as the arrangement of the cables for these sensors. The cables for the arc-weldable strain gauges installed at the pile heads were collected from the top of the pile cap and then merged with the cables from the other sensors (sister-bar type and concrete-embedded type) installed in the bridge pier. All the cables were organized along the vertical rebars in the bridge pier, exiting at the top of the hammer-head pier cap for data collection. To date, more than 2 years have passed since the installation of the sensors. All sensors are working perfectly well due to the careful installation procedures followed and protection measures taken during the instrumentation work.



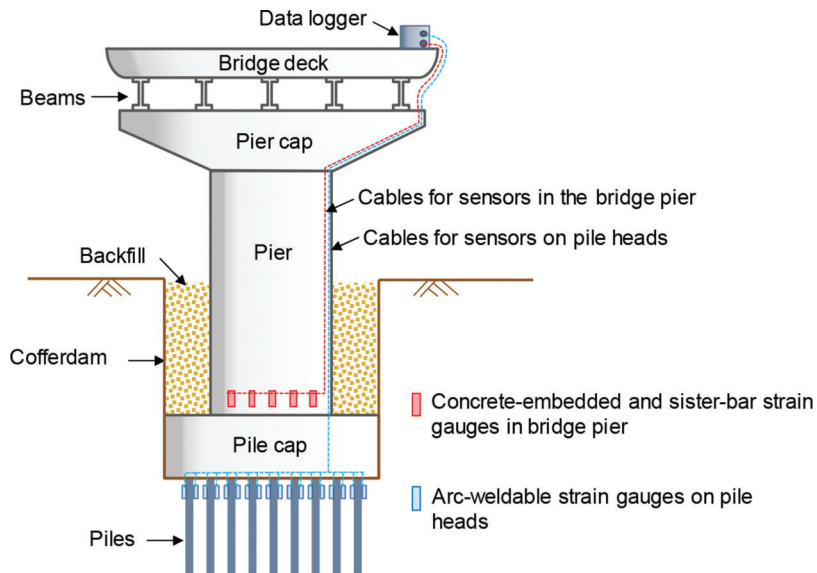
**Figure 3.4** Installation of the arch-weldable VW strain gauges on the pile head: (a) components of the strain gauge and (b) protection of the strain gauge.

TABLE 3.1  
Gauge factors for the sensors used in the bridge pier and on the pile heads

Gauge Type	Rebar (sister-bar) VW Gauge	Concrete-Embedded VW Gauge	Arc-Weldable VW Gauge
Model Number	4911	4200	4000
Gauge Factor ( $\mu\epsilon/\text{digit}$ )	0.354	3.304	4.062



**Figure 3.5** Strain gauge cable arrangement and protection: (a) arrangement of the gauge cables along the reinforcement rebars in the pile cap and (b) protection of the gauge cables using polyethylene foam.



**Figure 3.6** The structural and foundation components of pier 7, the locations of the sensors installed in the bridge pier and on the foundation elements, and the arrangement of the sensor cables.

#### 4. MEASUREMENT OF THE DEAD LOADS FROM THE BRIDGE

Load and settlement measurements for pier 7 of the Sagamore Parkway Bridge over the Wabash River have been periodically taken throughout the bridge construction stages and after the bridge construction was completed. In this chapter, we present the results of the measurements of the settlement of the bridge pier with time, the loads transferred from the pier to the foundation elements, the load distribution among




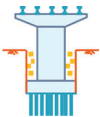
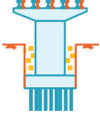

individual piles of the pile group supporting pier 7 and the load bearing capacity of the pile cap. In addition, we compare the load-settlement response of the production piles (in a  $3 \times 5$  group configuration) with that of the single, open-ended pile tested for project SPR-4040.

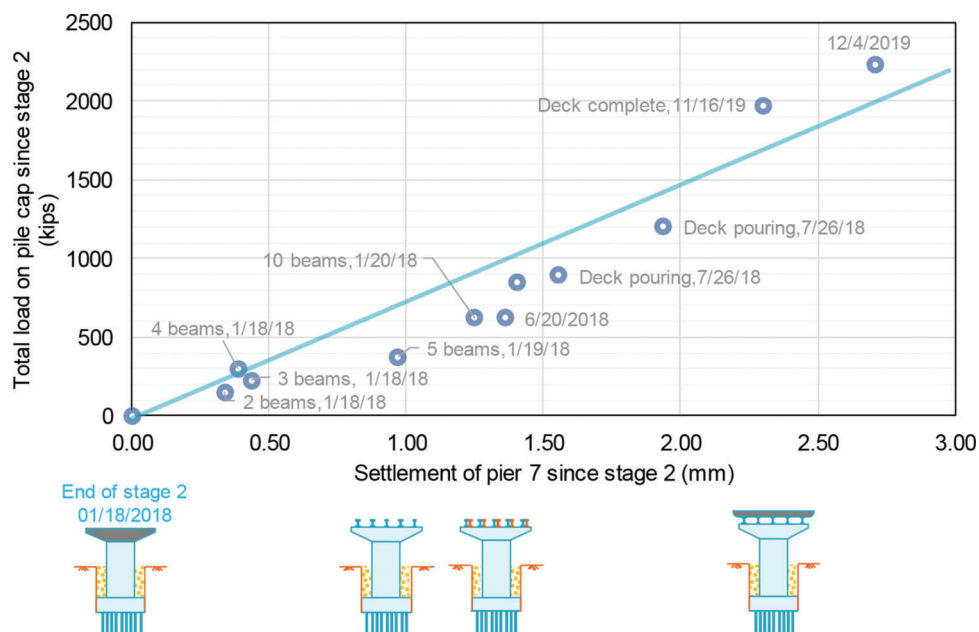
##### 4.1 Construction Stages

As summarized in Table 4.1, the construction of pier 7 took place in 5 stages: construction of the pier



TABLE 4.1  
Construction stages of pier 7 of the Sagamore Parkway Bridge over Wabash River

Stage	Description	Illustration	Time Period
0	Pile driving and pile cap construction		11/15/2016 to 12/4/2017
1	Construction of pier column		12/4/2017 to 12/12/2017
2	Backfilling of the cofferdam and pier cap pouring		12/12/2017 to 1/18/2018
3	Placement of beams over the span between pier 7 and bent 8		1/18/2018 to 1/19/2018
4	Placement of beams over the span between pier 6 and pier 7		1/19/2018 to 1/20/2018
5	Construction of the bridge deck		1/20/2018 to 9/16/2018



**Figure 4.1** Total load applied on the pile cap versus the corresponding settlement of pier 7 measured at different stages during and after bridge construction.

column, backfilling of the cofferdam and pier cap pouring, placement of the deck beams over the span between pier 7 and bent 8 (refer to Figure 1.1),

placement of deck beams over the span between pier 6 and pier 7, and construction of the bridge deck. The measurements of loads in the piles started when the

construction of the pile cap was completed on December 4, 2017. The strain readings taken that day were used as the zero reference for subsequent strain readings. Therefore, stage 0 consists of the driving of the piles and the construction of the pile cap. The construction of the bridge took about 2 years; the bridge was opened to traffic on September 16, 2018.

#### 4.2 Load-Settlement Curve

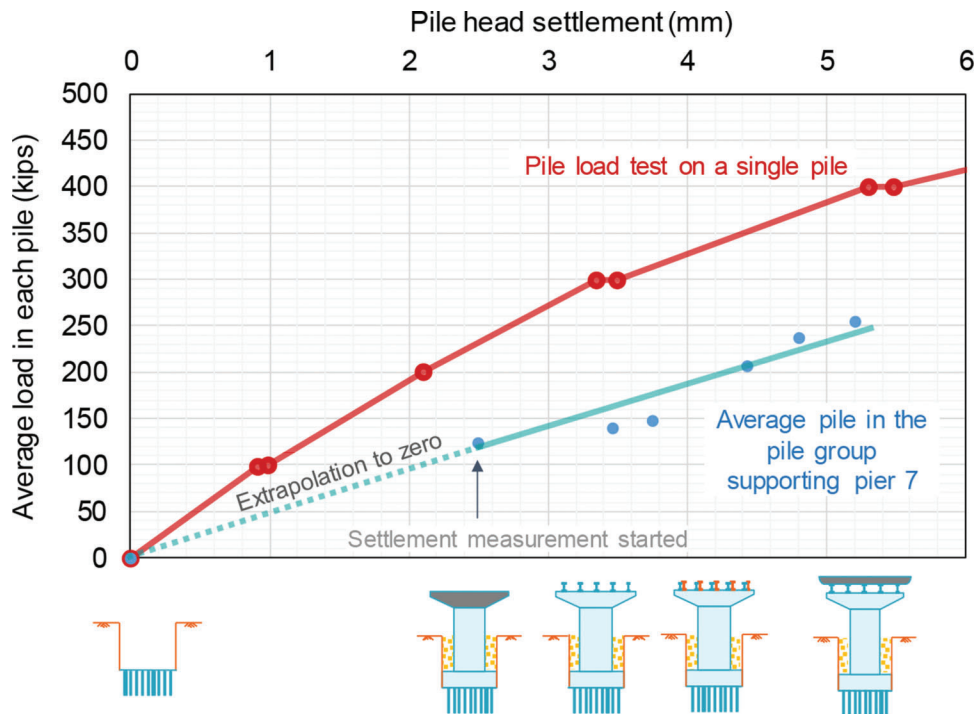
Due to limited accessibility to the bridge pier during construction stages 1 and 2, the barcode polymer sticker used for settlement measurements was attached to the bridge pier (see Figure 3.1b) about 5 ft above the ground surface on January 18, 2018, after the “hammer-head” pier cap (see Figure 3.6) was constructed. Since then, periodical measurements have been taken to monitor the settlement of pier 7 during and after the bridge construction. From January 18, 2018, to March 17, 2020, a total settlement of 2.7 mm was measured for pier 7.

Figure 4.1 shows the total load applied in stages on top of the pile cap versus the corresponding settlement of pier 7 since completion of stage 2 (construction of the pier cap and backfilling of the cofferdam). Illustrations of the corresponding construction stages are shown for reference below the load-settlement curve in Figure 4.1. The load-settlement response of pier 7 from the end of stage 2 to the end of the bridge construction is almost linear.

Figure 4.2 shows the average load-settlement response of the production piles under pier 7. The load-settlement curve was obtained by plotting the

average vertical load measured at the heads of the piles in the group versus the pile head settlement (the assumption is that the bridge pier, the pile cap and all the piles in the group settled by the same amount). Because the settlement measurements started only after the pier cap was constructed (on January 18, 2018), any pile head settlement that took place before that date was estimated by extrapolating the average pile head load-settlement curve obtained after January 18, 2018, back to the origin (corresponding to zero load on the piles) by assuming a linear load-settlement response (shown as the dashed line in Figure 4.2). This way, a total pile head settlement of 5.2 mm was obtained for the piles under pier 7 from November 15, 2016 to March 17, 2020.

Based on observations and measurements made on hundreds of bridges in Canada and the United States, tolerable vertical movements for bridge foundations have been proposed (Bozozuk, 1978). Vertical movements less than 50 mm were classified as tolerable, vertical movements between 50 and 100 mm were deemed harmful but tolerable, and vertical movements greater than 100 mm caused heavy damage to the bridge structures, and hence, were classified as intolerable. Similar observation-based studies were also performed by other researchers. Table 4.2 summarizes the settlement criteria for bridge piers and foundations. AASHTO (2018) prescribes allowable angular distortion criteria to prevent serviceability limit states from being reached; the angular distortion should be less than 0.004 for continuous-span bridges and less than 0.008 for simple-span bridges. This means that the



**Figure 4.2** The load-settlement curve of the test pile obtained from the pile load test performed in 2016 and that of an average production pile in the 3 × 5 pile group under pier 7 of the Sagamore Parkway Bridge over the Wabash River.



TABLE 4.2  
The settlement criteria for bridge piers and foundations in the literature

Reference	Settlement Range	Description of Condition
Bozozuk (1978)	$w < 50$ mm $50 \text{ mm} < w < 100$ mm $w > 100$ mm	Tolerable Harmful but tolerable Intolerable: heavy damage to the bridge structures
Grover (1978)	$w < 25$ mm $50 \text{ mm} < w < 70$ mm $w > 100$ mm	Tolerable: no damage Minor damage Significant structural damage to the bridges
Walkinshaw (1978)	$w > 63$ mm	Poor riding conditions

allowable differential settlement of the Sagamore Parkway Bridge (a continuous-span bridge) is 112 mm ( $= 92 \text{ ft} \times 0.004$ ) for the span over pier 6 and pier 7 and 161 mm ( $= 132 \text{ ft} \times 0.004$ ) for the span over pier 7 and bent 8. The total settlement of a pier must be greater than or equal to the differential settlement between the pier and its neighboring pier (assuming that none of the piers are moving upward). Based on the allowable angular distortion prescribed by AASHTO (2018), the allowable total settlement for pier 7 is at least 112 mm (the smaller of 112 mm and 161 mm), which is greater than the tolerable total vertical settlement recommended by the references summarized in Table 4.2. At a settlement level of 10% of the pile diameter, ultimate limit states are reached for piles (Han, Prezzi, et al., 2017; Jardine, Chow, Overy, Standing, & Jamie, 2005; Kolk et al., 2005; Lehane et al., 2005; Salgado, 2008). This corresponds to 61 mm ( $= 10\% \times 610 \text{ mm}$ ) for the piles supporting pier 7. The total settlement of the piles under pier 7, measured from pile installation (November 15, 2016) to the last measurement (March 17, 2020), was 5.2 mm, which is minimal compared with any of the settlement criteria mentioned above.

A slow-maintained static load test was performed in 2016 on a single, instrumented open-ended pipe pile next to pier 7 to provide guidance for the design of the production piles of the Sagamore Parkway bridge. The load-settlement curve obtained from the static load test is also plotted in Figure 4.2 for comparison. The load-settlement stiffness of the open-ended test pile decreases slightly with increasing settlement, whereas the average load-settlement curve for a pile in the group supporting pier 7 is almost linear. The secant stiffness (the slope from the origin of the load-settlement space to the point on the curve being considered) of the single pile calculated for a settlement level of 5 mm is 76.4 kips/mm, which is about 1.65 times of that ( $= 46.4 \text{ kips/mm}$ ) of an average pile in the  $3 \times 5$  pile group. This is consistent with the findings in the literature (Han et al., 2015; Han, Salgado, et al., 2019; Salgado et al., 2017) that the initial load-settlement stiffness of an average pile in a pile group is significantly smaller than that of a single pile installed in the same soil profile. However, the load-settlement stiffness of a single pile quickly decreases as the shaft resistance mobilization stabilizes after reaching its limit value (limit shaft resistance  $Q_{sL}$ ),

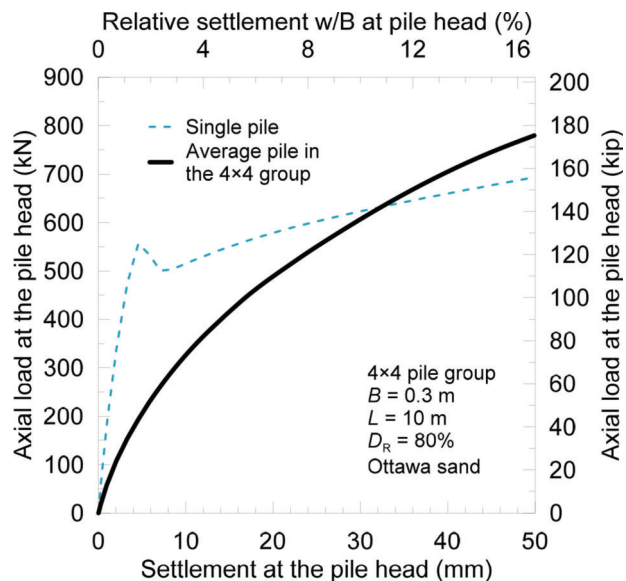
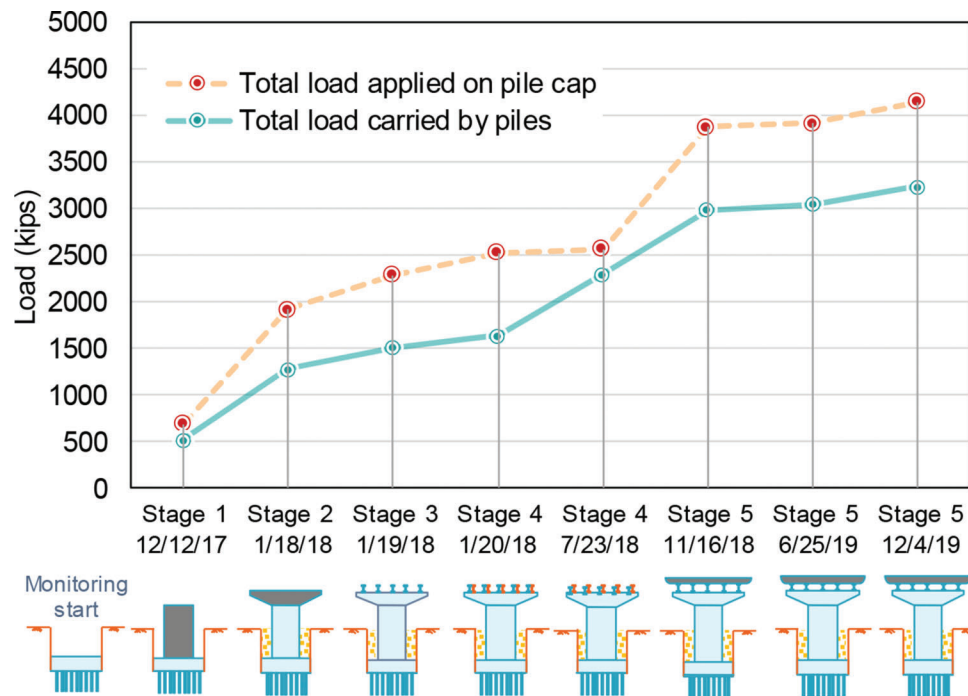


Figure 4.3 The load-settlement curves of a single pile and an average pile in a  $4 \times 4$  pile group in dense sand ( $D_R = 80\%$ ) (after Han, Salgado, et al., 2019).

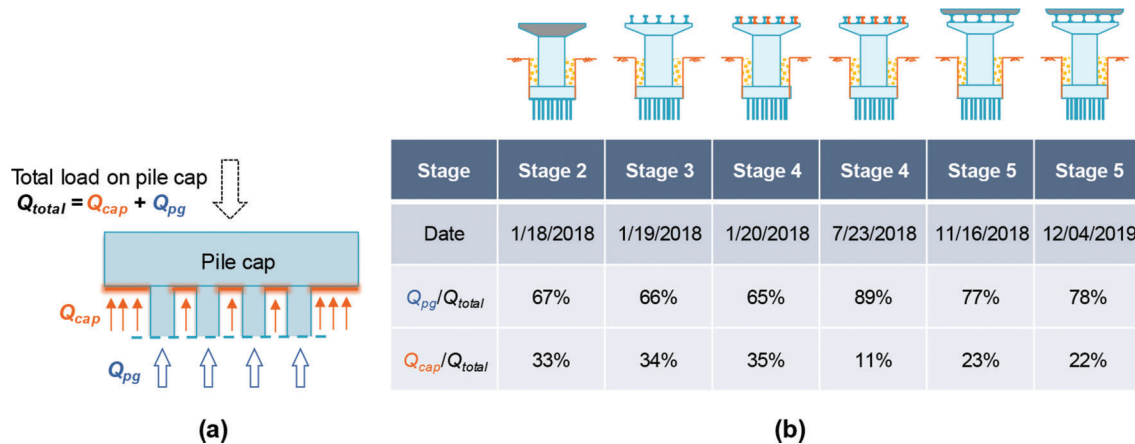
whereas the average resistance of the piles in a pile group increases continuously, exceeding that of the single pile at a large settlement level (e.g., 30 mm–50 mm for a  $4 \times 4$  pile group, as shown in Figure 4.3).

#### 4.3 Load Transfer from the Superstructure to the Foundation

The dead and live loads coming from the superstructure are transferred through the bridge pier to the pile cap and then to the piles. With the readings collected from the sensors installed in pier 7 and all the fifteen piles supporting it, the load transfer from the superstructure to the foundation elements was obtained at different stages during and after the bridge construction. Figure 4.4 compares the history of the total load (shown as the dashed orange line) on top of the pile cap with the total load (shown as the solid blue line) carried by the pile group. The corresponding dates of the measurements and the sketches of the construction stages are shown below the figure for reference. The total vertical load on the pile cap consists of two



**Figure 4.4** Total load applied on the pile cap and total load carried by the piles in the group measured at different stages during and after the bridge construction.

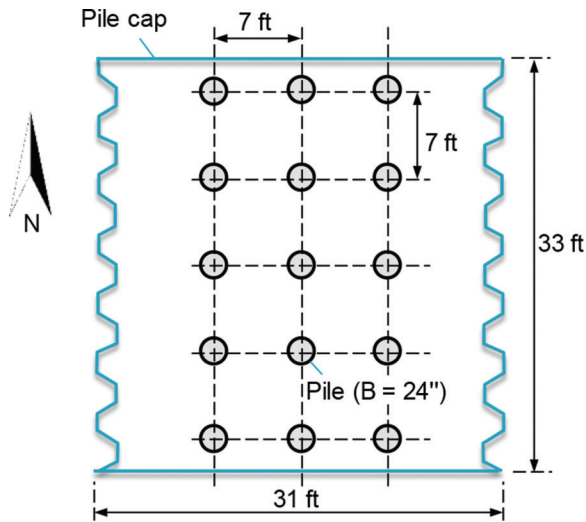


**Figure 4.5** Contribution of the pile cap to the bearing capacity of the pile group: (a) the equilibrium of forces applied on the pile cap and (b) the  $Q_{pg}/Q_{total}$  and  $Q_{cap}/Q_{total}$  ratios obtained at different stages.

components: the vertical load coming from the superstructure through the bridge pier and the gravity load of the backfill in the cofferdam. The axial load in the bridge pier was obtained from the sensors installed near the bottom of the pier column (as shown in Figure 3.6), whereas the gravity load of the backfill was estimated to be 1,049 kips based on the volume and unit weight (assumed to be 110 pcf = 17.3 kN/m<sup>3</sup>) of the backfill.

Considering the equilibrium of the pile cap, as shown in Figure 4.5a, the total load  $Q_{total}$  on top of the pile cap is balanced by the load  $Q_{pg}$  carried by all the fifteen piles in the pile group and the load  $Q_{cap}$  carried by the soil under the pile cap. Thus, the difference between the two curves (representing  $Q_{total}$  and  $Q_{pg}$ ) shown in

Figure 4.4 is equal to the load carried by the soil below the pile cap, which is also the cap resistance  $Q_{cap}$ . Figure 4.5 summarizes the  $Q_{pg}/Q_{total}$  ratio and the  $Q_{cap}/Q_{total}$  ratio for all the bridge construction stages. Although the majority of the superstructure loads are carried by the piles,  $Q_{cap}$  takes a significant share of the total load (23% at the end of the bridge construction). Currently, the pile cap resistance  $Q_{cap}$  is not considered in INDOT bridge designs. Accounting for this additional load-bearing component in bridge foundation design can potentially lead to significant savings of materials and construction time. This additional capacity could be considered particularly in bridge replacement and rehabilitation projects.

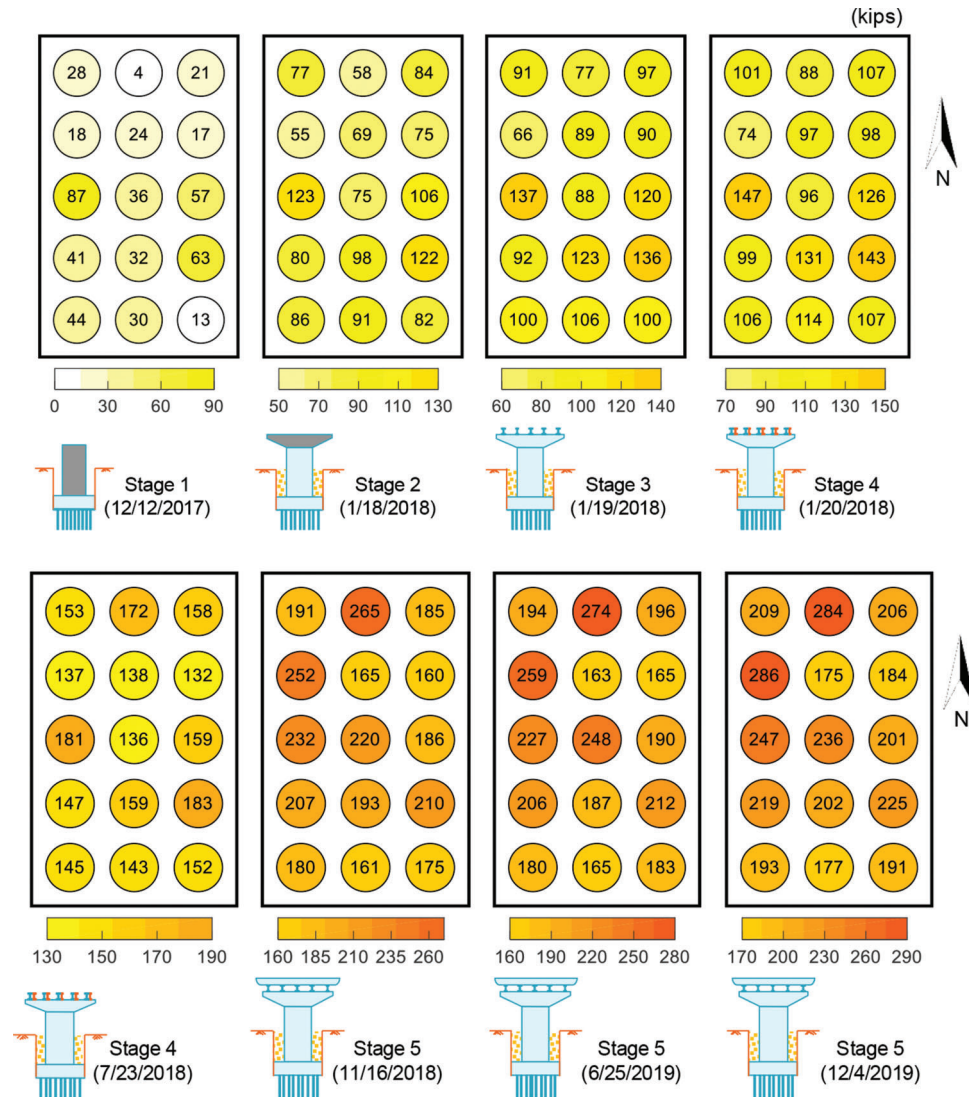


**Figure 4.6** Layout of the pile group and cross section of the pile cap under pier 7.

Figure 4.6 shows the layout of the  $3 \times 5$  pile group of pier 7 and a cross section of the pile cap. The pile cap has a cross-sectional area of about  $1,023 \text{ ft}^2$  and a thickness of 7 ft. The total cross-sectional area of the fifteen piles (with a diameter of 24 inches) is about  $47.1 \text{ ft}^2$ , corresponding to only 4.6% of the entire cross-sectional area of the pile cap. The remaining 95.4% of the area of the pile cap is supported by the soil under it. This partly explains the large cap resistance  $Q_{\text{cap}}$  measured in the present study.

#### 4.4 Distribution of the Dead Loads Among Piles in the Group

A pair of vibrating-wire strain gauges were installed on each of the fifteen piles supporting pier 7, as described in Chapter 3. With the strain readings collected from these sensors, the load distribution among the individual piles in the  $3 \times 5$  pile group was obtained at different stages during and after the construction of the bridge. As shown in Figure 4.7, with a few exceptions,



**Figure 4.7** Distribution of dead loads among piles in the group at different stages during and after bridge construction.

the loads carried by the individual piles in the group were approximately evenly distributed throughout the construction stages. According to Han, Salgado, et al. (2019), the load-settlement response of individual piles in a pile group are similar at small pile-head settlement levels ( $< 5$  mm) because the pile group and the surrounding soil settle as a block in the beginning of loading. As loading continues and the settlement increases, the difference in the load response of the individual piles in the group becomes prominent: the corner and edge piles tend to develop resistance faster than the center piles, whereas the center piles have the potential to develop greater bearing capacity at larger settlement levels.

## 5. LIVE LOAD TEST

In order to study the response of the bridge pier and its foundation elements to live loads, a live load test was performed between March 19, 2019, and March 20, 2019 (Han, Marashi, et al., 2020). With the bridge temporarily closed to traffic, twelve fully-loaded triaxle trucks were used to apply the live loads. In this chapter, we present and discuss the results of the live load test: the bridge load-settlement response, the load transferred from the pier to the pile group, the load eccentricity, and the load distribution in the bridge pier and among the fifteen piles in the group.

### 5.1 Test Procedure

#### 5.1.1 Load Steps

The live load test was performed in seven load steps by parking loaded triaxle trucks in sequence at specified locations on the bridge deck near pier 7, as illustrated in Figure 5.1. The weights of the trucks are provided in Table 5.1; the average truck weight was 53 kips. Table 5.2 summarizes the number of trucks parked at each location during the seven load steps of the live load test. At each specified location (A, B, C, D, or E), three

trucks were parked side-by-side with equal spacing (about 4 ft) between them to maximize the applied loads, as shown in Figure 5.2b. The load sequence prescribed in Table 5.2 was intended to simulate a number of loaded trucks approaching pier 7, driving over pier 7, and then leaving the bridge. The load step with a group of 12 loaded trucks parked on the bridge deck near pier 7 at the same time (i.e., load step 4) resulted in the largest load in the pier, representing an extreme loading condition. The trucks were driven at a speed of 5–10 mi/hr to reach the specified locations where they remained parked during testing. After each load step was applied, the settlement of the pier was measured at five-minute intervals. Only when the pier settlement stabilized (with two consecutive settlement readings being the same), the next load step was applied. Each load step lasted about 30 minutes on average. As shown in Figure 5.2, high-intensity LED work lights were used to illuminate the barcode sticker on the bridge pier for settlement measurements since the live load test was performed at night to minimize traffic disruption. The strain readings were collected continuously from the sensors installed in the bridge pier and on the pile heads to obtain the load histories in the pier and piles throughout the live load test.

#### 5.1.2 Eccentricity of the Live Load

Figure 5.3(a) and (b) show the top view and side view, respectively, of the locations of the trucks that were used to apply the live loads on the bridge deck.

TABLE 5.1  
The weight (in kips) of the twelve trucks used for the live load test (refer to Figure 5.1 for the locations of the trucks)

Location B	Location C	Location D	Location E
51.5	51.5	51.6	56.4
53.0	51.2	52.4	51.7
51.9	51.0	56.5	58.2

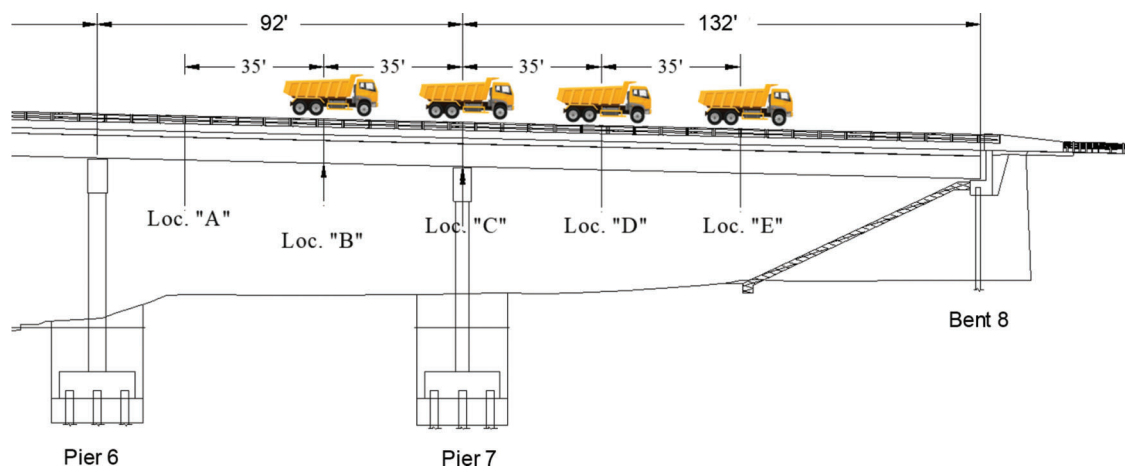


Figure 5.1 Locations on the bridge deck where the live loads were applied (the configuration for load step 4 is shown in the figure).



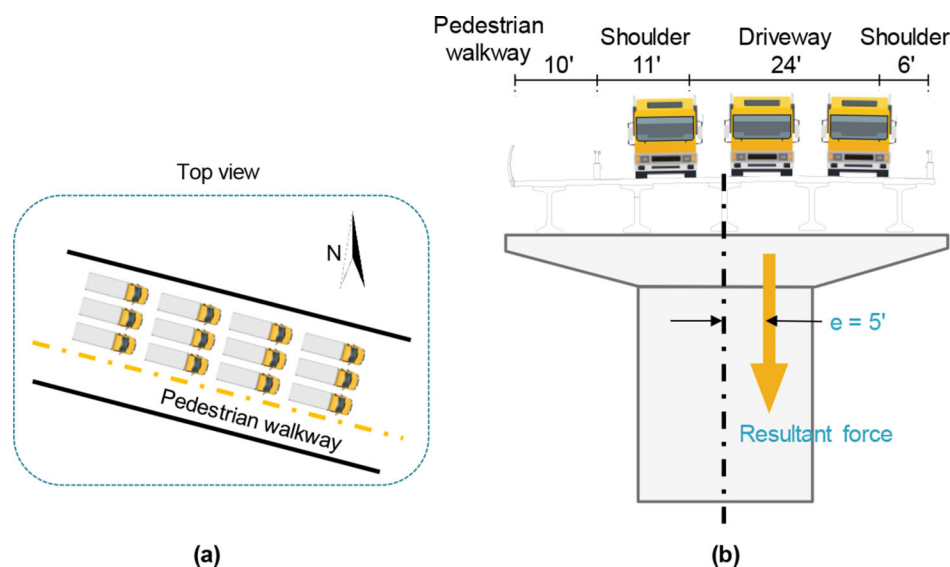
TABLE 5.2

The numbers of trucks positioned at the specified locations on the bridge deck in each load step during the live load test

Load Step	Number of Trucks				
	Location A	Location B	Location C	Location D	Location E
0	—	—	—	—	—
1	3	3	—	—	—
2	3	3	3	—	—
3	3	3	3	3	—
4	—	3	3	3	3
5	—	—	3	3	3
6	—	—	—	3	3
7	—	—	—	—	—



**Figure 5.2** Live load test in progress: (a) settlement measurement for pier 7 and (b) loaded trucks on the bridge deck applying the live loads.



**Figure 5.3** Live loads applied on the bridge: (a) top view of the bridge deck with the trucks that were used to apply the live loads and (b) cross section of the bridge at pier 7 and the eccentricity of the resultant live load.

Because of the safety barrier that separates the pedestrian-walk lane from the traffic lanes, only three trucks can be parked side-by-side in a row in the traffic lanes. Consequently, the resultant force applied by the

trucks was eccentric (towards the north side of the bridge deck, as shown in Figure 5.3a) with respect to the neutral axis of the bridge pier. Based on the dimensions shown in Figure 5.3b, the eccentricity



(the distance from the resultant force to the neutral axis of the bridge pier) is estimated to be 5 ft (1.52 m).

## 5.2 Test Results

The strain readings were collected continuously from the strain gauges and then used to calculate the axial loads in the bridge pier and at the heads of all fifteen piles in the group supporting the pier at each load step. The strain readings taken at load step 0 (corresponding to no trucks on the bridge deck) were used as the zero reference, and all the load measurements presented in this chapter resulted from the live load applied by the trucks on the bridge deck.

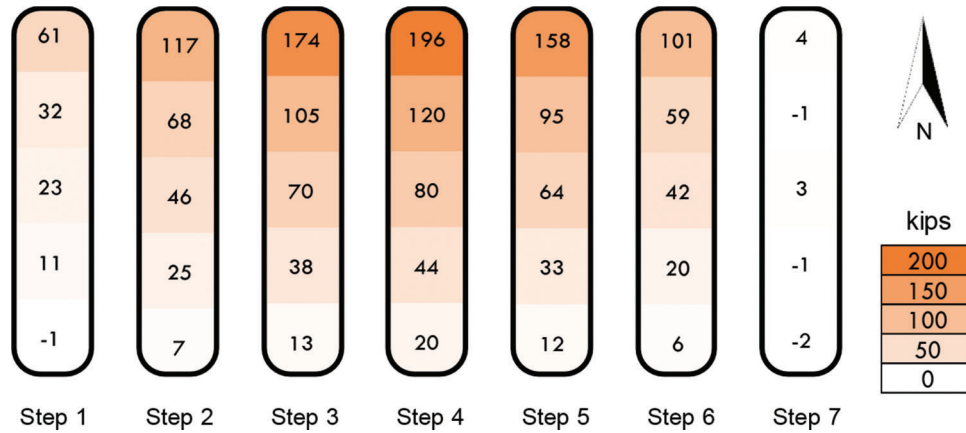
### 5.2.1 Load in the Bridge Pier

As shown in Figure 5.4, the cross section of the bridge pier can be divided into 5 regions, with three strain gauges (two rebar and one concrete-embedded strain gauges) installed in each region. The strain readings obtained from the three strain gauges in each

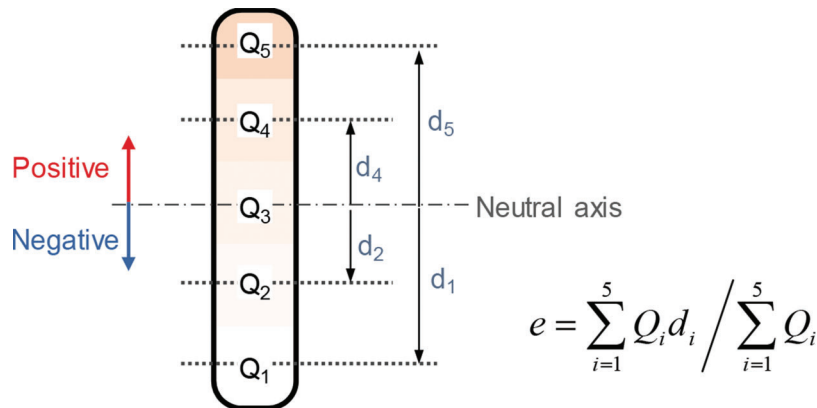
region were used to calculate the axial force resulting over that region. Figure 5.4 shows the distribution of the axial loads induced only by the live loads within the cross section of the bridge pier at each load step. As expected, the axial loads on the northern end of the pier were greater than those on the southern end due to the eccentricity of the resultant live load (Figure 5.3). The eccentricity  $e$  of the resultant live load over the cross section can be calculated as:

$$e = \frac{\sum_{i=1}^5 Q_i d_i}{\sum_{i=1}^5 Q_i} \quad (\text{Equation 5.1})$$

where  $Q_i$  is the axial load in the  $i_{th}$  region and  $d_i$  is the distance measured from the center of the  $i_{th}$  region to the neutral axis of the bridge pier. Figure 5.5 shows how the resultant live load eccentricity  $e$  was calculated. The distance  $d_i$  is positive above the neutral axis, and so is the calculated eccentricity  $e$ . Using the data shown in Figure 5.4, the calculated resultant live load eccentricity ranges from 5.0 ft to 6.2 ft (1.52 m–1.89 m) for all the load steps; these values are in agreement with



**Figure 5.4** Live load distribution over the cross section of the bridge pier at each load step during the live load test.



**Figure 5.5** Calculation of the eccentricity  $e$  of the resultant live load. The distance  $d_i$  is positive above the neutral axis and negative below the neutral axis.

the eccentricity ( $= 5 \text{ ft} = 1.52 \text{ m}$ ) estimated based on the location of the trucks and the geometry of the bridge deck (see Figure 5.3), highlighting the high quality of the load measurements.

As the trucks drove towards pier 7, the loads in the pier increased gradually (Figure 5.4), peaking at step 4 when all twelve trucks were located close to pier 7 (shown in Figure 5.1 and Table 5.2). As the trucks drove away from the pier, the live loads in the pier decreased, returning to nearly zero at step 7 when all trucks were off the bridge. We emphasize that the loads shown in Figure 5.4 are load increments with respect to step 0 (with no trucks on the bridge), representing only the live loads applied by the trucks parked on the bridge. The total axial live load in the pier can be calculated by summing up the axial forces in the five regions within the cross section of the pier. The maximum live load (at step 4) in the pier was 460 kips (2,046 kN). The dead load (resulting from the structural weight) carried by this pier was measured to be 2,830 kips (12,588 kN), leading to a ratio of 16% between the live load and the dead load under these conditions.

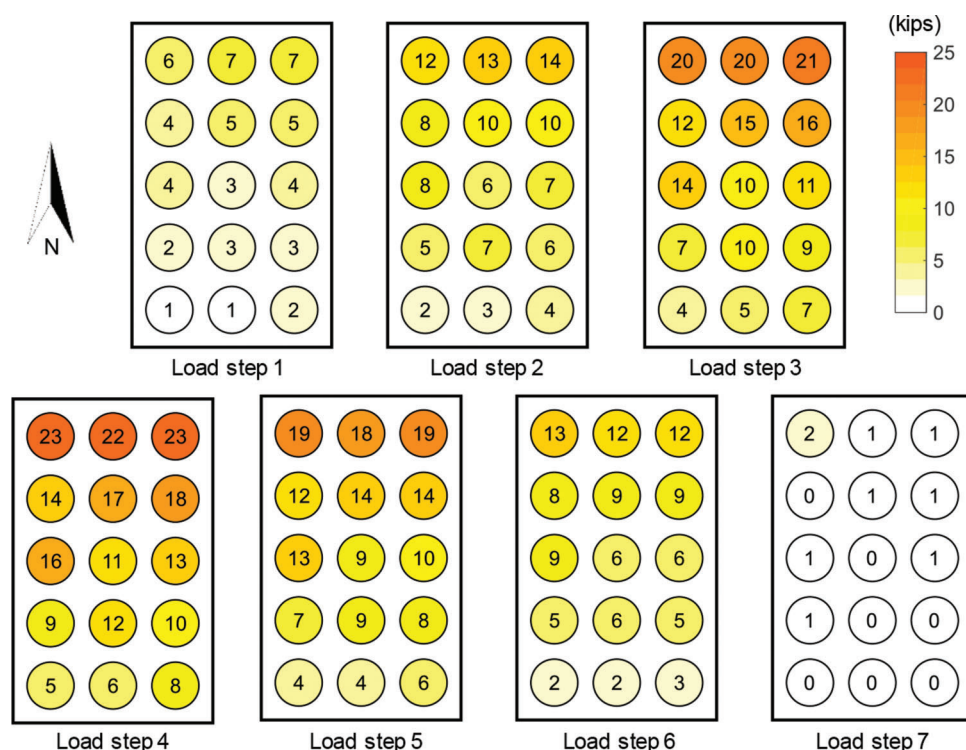
### 5.2.2 Load Distribution Among Piles in the Group

Figure 5.6 shows the distribution of the live loads among the fifteen piles in the  $3 \times 5$  pile group at each load step during the live load test. As a result of the eccentricity of the applied live loads (see Figure 5.3), the axial loads in the piles gradually increased from the south side to the north side at each load step. This is

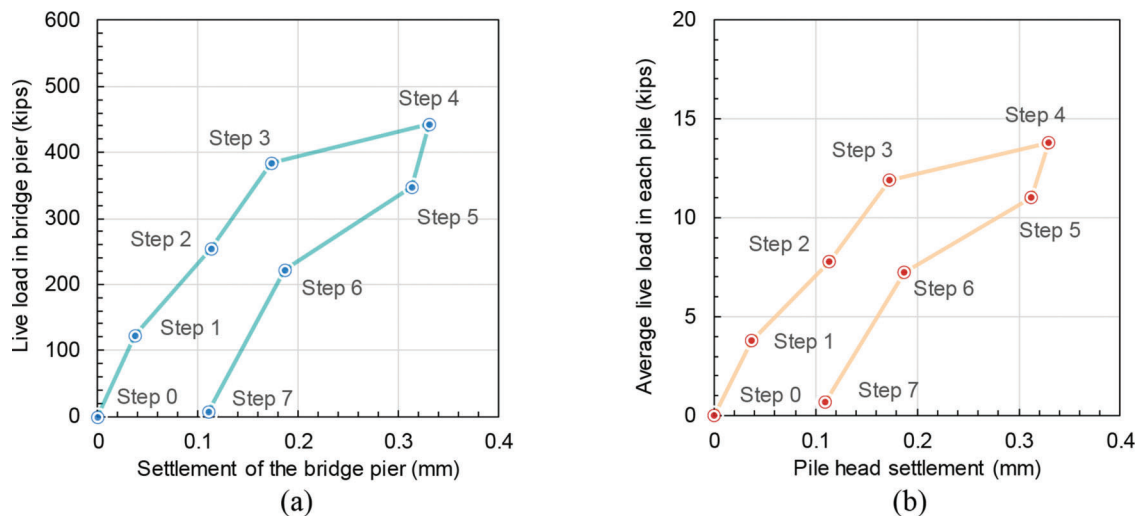
consistent with the load history seen in the bridge pier (in Figure 5.4). The loads in the piles increased as the trucks were driven toward the pier and parked at their specific locations in each load step. Peak loads on the piles were reached at load step 4; the loads decreased to nearly zero as the trucks left the bridge.

### 5.2.3 Load-Settlement Response and Load Transfer Behavior

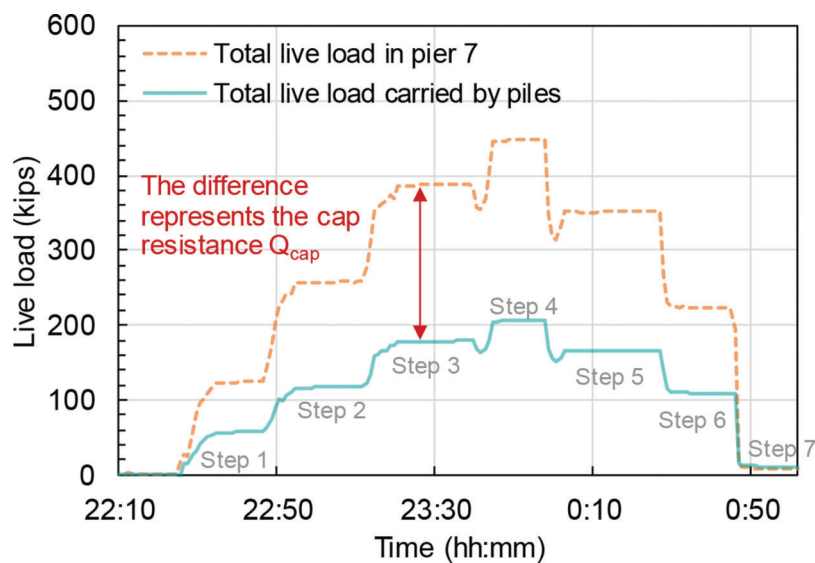
The settlement of the bridge pier was measured at each load step using a digital level, as described in Chapter 3. Figure 5.7a shows the load-settlement response of the bridge pier obtained from the live load test. The maximum settlement was measured to be less than 0.4 mm at load step 4, during which the live load level was maximum. Assuming that the settlement at the pile heads was the same as the settlement of the bridge pier, the load-settlement curve for an average pile in the  $3 \times 5$  pile group is plotted in Figure 5.7b. The secant load-settlement stiffness of an average pile in the group calculated from zero live load (load step 0) to the maximum live load level (load step 4) is 42.4 kips/mm. This is slightly less than that ( $= 46.4 \text{ kips/mm}$ ) obtained from the dead loads applied during bridge construction, resulting in a settlement of 5 mm, as discussed in Section 4.2. There was a small (about 0.1 mm) residual settlement at the end of the live load test (see Figure 5.7); this may be simply due to a measurement error since the settlement measurement accuracy of the digital level is submillimeter.



**Figure 5.6** Distribution of the live loads at the heads of the fifteen piles in the group at different load steps during the live load test.



**Figure 5.7** Load-settlement curve: (a) for the bridge pier and (b) for an average pile in the group.



**Figure 5.8** The live load in the bridge pier (pier 7) versus the total load carried by all the piles during the live load test.

Figure 5.8 shows the history of total loads in the bridge pier and in the piles during the live load test. The total load carried by the bridge pier was greater than that carried by the piles, and the difference between these loads was the load carried by the soil immediately in contact with the pile cap (a force equilibrium diagram is shown in Figure 4.5a). Taking load step 4 as an example, about 50% of the live load in the bridge pier was transferred to the piles, while the remaining 50% of the live load was carried by the soil under the pile cap. In contrast, about 80% of the dead load from the superstructure was transferred to the piles, and the remaining 20% was carried by the soil under the pile cap during the bridge construction stages (see Chapter 4). When the live loads were applied in a short period of time (less than 30 minutes) during the live load test, then a greater portion (about 50%) of the live load

was first carried by the pile cap. Gradually, some of the load carried by the pile cap was transferred to the piles, as observed during stage 4 of bridge construction from January 20, 2018, to July 23, 2018 (see Figure 4.4). The ratio of the load  $Q_{cap}$  carried by the soil below the pile cap to the total superstructure load  $Q_{total}$  applied on the pile cap stabilized at 22% after the bridge construction was completed (the value changed from 23% to 22% from November 16, 2018, to December 4, 2019).

## 6. DESIGN OF BRIDGE FOUNDATIONS

### 6.1 Comparison Between the Design Loads and Measured Loads

The average dead load per pile under pier 7 was measured as 248 kips at the completion of the bridge

construction (measured on November 16, 2018). In comparison, the dead load was estimated to be 336 kips per pile in the bridge design, which is 41% greater than the measured dead load. However, the cap resistance  $Q_{cap}$  was assumed to be zero in the bridge design, meaning that all the load from the superstructure would be carried by the piles. In contrast, the load measurement in the present study shows that the piles under pier 7 carried about 77% (= 3,725 kips) of the total superstructure load (= 4,869 kips) from the pier, and the remaining 23% of the total load (1,145 kips) was carried by the pile cap. If we assuming that the cap resistance was zero, this produces a total dead load of 4,869 kips to be carried by the group piles, resulting in an average load of 325 kips per pile (=  $4,869/15 = 325$  kips). This average load per pile is in good agreement with the unfactored design dead load of 336 kips. This means that the dead loads used in the bridge design were satisfactory estimates of the real values of the dead loads.

The maximum axial live load carried by a pile in the group under pier 7 was measured as 23 kips at load step 4 during the live load test (as reported in Chapter 5). As revealed by the data obtained from the live load test (see Chapter 5), a large portion (about 50%) of the live loads were carried by the pile cap. In addition, due to the eccentricity of the live loads applied by the twelve trucks on the bridge deck, a bending moment about the center of the pile cap was applied on the pile cap. For example, in load step 4 of the live load test, an axial load of 460 kips and a bending moment of 2,300 kips-ft resulting from the truck loads were applied on the pile cap. The fifteen piles under the pile cap carried about 207 kips of the axial load and 822 kips-ft of the bending moment, and the remaining 253 kips of the axial load and 1478 kips-ft of the bending moment were carried by the soil below the pile cap. Assuming that the pile cap did not carry any load (to be consistent with the bridge design assumptions) and applying the entire axial load (= 460 kips) and bending moment (= 2,300 kips-ft)

resulting from the truck loads at load step 4 (an extreme traffic scenario) to the piles in the group, the maximum live load carried by a pile in the group is calculated as 53 kips.

The live load test was modeled by Parsons Corporation using the bridge analysis software LEAP Bridge Concrete using the same truck weights and locations as specified in the live load test. By assuming a continuous-span bridge, a maximum unfactored live load of 545 kips in pier 7 and a maximum unfactored live load of 62 kips in a pile under pier 7 were obtained from the structural analysis of the live load test. If a simple-span assumption is used in the simulation, the maximum unfactored live loads in the pier and in the pile are 443 kips and 51 kips, which are less than obtained with the continuous-span assumption. The maximum live load (= 23 kips) in a pile measured during the live load test is smaller than those (62 kips or 51 kips) obtained from the simulations, using either continuous-span or simple-span assumptions. This is because a significant portion of the applied live load (and the resulting bending moment) was carried by the soil below the pile cap during the live load test. The maximum live load (= 53 kips) in a pile supporting pier 7, corrected for the pile cap resistance (as described above), is in close agreement with the simulation loads (62 kips and 51 kips) obtained using the continuous-span and simple-span assumptions.

The unfactored live load considered in the design of the production piles was 185 kips; it consists of the vehicular live load, water load and stream pressure, wind on live load, wind load on structure, and friction load. Out of this 185 kips of live load, 81 kips is the vehicular live load, which is less than half of the total live load considered in single pile design. These values are summarized in Table 6.1.

The live loads were applied statically by parking the trucks at specified locations on the bridge deck during the live load test. This is different from the scenario in which the trucks are being driven over the bridge deck

TABLE 6.1  
Maximum live loads for pier 7 and for the piles supporting it, according to different approaches

Item	Approach	Maximum Live Load in Pier 7 (kips)	Maximum Live Load for a Pile Under Pier 7 (kips)	Notes
Live load used in pile design	LEAP	–	185	Vehicular live load, water load and stream pressure, wind on live load, wind load on structure, and friction load
Live load according to AASHTO (2018)	LEAP	–	81	Only vehicular live load
Simulation of live load test–1	LEAP	545	62	Assuming a <i>continuous-span</i> bridge
Simulation of live load test–2	LEAP	443	51	Assuming a <i>simple-span</i> bridge
Measured live load during live load test	Measurement	460	23	Direct measurement from the sensors
Measured live load during live load test (corrected for pile cap resistance)	Measurement	460	53	Assuming the entire live load is carried by the piles (neglecting any capacity contribution from the pile cap)





**Figure 6.1** Static pile load test performed on instrumented open-ended test pile at the Sagamore Parkway Bridge site (after Han, Ganju, Salgado, & Prezzi, 2019).

at some speed. To account for the dynamic effect of moving vehicles on the bridge response, AASHTO (2018) prescribed a dynamic factor  $1+IM$  to be applied to the static loads, where  $IM$  (an abbreviation for impact) is the dynamic load allowance. In the design of bridge piers,  $IM$  is taken as 0.33, meaning that a dynamic factor of 1.33 needs to be applied to the static live loads calculated as prescribed in AASHTO (2018). However, for foundation elements below the ground surface,  $IM$  is equal to 0 and the dynamic factor is equal to 1, implying that the dynamic effect of the moving vehicles on the bridge is not experienced by the foundation elements.

## 6.2 LRFD Design of the Bridge Foundations

During the bridge design phase, slow-maintained static load tests (as shown in Figure 6.1) were performed on two heavily-instrumented test piles—one closed-ended and the other open-ended—to provide guidance in the design of the production piles for the interior piers and the end bents of the Sagamore Parkway Bridge (Ganju et al., 2020; Han, Ganju, Prezzi, et al., 2020; Han, Ganju, Salgado, et al., 2020). The high-quality data collected from the static load tests yielded the unit shaft resistance  $q_{sL}$  along the entire pile length (as summarized in Table 6.2) and unit base resistance  $q_b$  that were used in the design of the production piles.

The design of the production piles was performed following the Load and Resistance Factor Design (LRFD) framework, as prescribed by AASHTO (2018),

which requires the total factored resistance to be equal to or greater than the total factored load:

$$(RF_b Q_b^n + RF_s Q_{sL}^n) \eta_g \geq LF_{DL} DL^n + LF_{LL} LL^n \quad (\text{Inequality 6.1})$$

where  $RF_b$  and  $RF_s$  are the resistance factors for the nominal base resistance  $Q_b^n$  and the nominal shaft resistance  $Q_{sL}^n$ , respectively.  $LF_{DL}$  and  $LF_{LL}$  are the load factors for the nominal dead load  $DL^n$  and nominal live load  $LL^n$ , respectively. According to Section 10.5.5.2.3 in AASHTO (2018), a resistance factor of 0.8 (for both  $RF_b$  and  $RF_s$ ) should be used if the nominal resistance is obtained based on static load test(s) on at least one pile and dynamic testing on at least two piles per site. The group efficiency factor  $\eta_g$  is equal to 1 for driven piles in sand, as specified in Section 10.7.3.9 of AASHTO (2018).

The unit shaft resistance  $q_{sL}$  of the open-ended production piles of the interior piers of the bridge at each elevation was assumed to be the same as that of the open-ended test pile obtained from the static load test (see Table 6.2). The unit shaft resistance  $q_{sL}$  was then integrated along the pile length to calculate the total nominal shaft resistance  $Q_{sL}^n$  of the production pile. Note that the shaft resistance above an elevation of 475 ft, the 100-year scour elevation, was ignored to account for the detrimental scour effect on the shaft resistance. Similarly, the unit annulus resistance  $q_{ann} = 21.2$  MPa and the unit plug resistance  $q_{plug} = 1.3$  MPa obtained from the static load test were

TABLE 6.2

Unit shaft resistance  $q_{sL}$  obtained from the static load test on the open-ended pipe pile

Elevation Range (ft)	Soil Description	Unit Shaft Resistance (ksf)	Gravel Content (%)	$q_c$ (ksf)	$q_{sL}/q_c$
522–513	Clayey silt with sand	0.11	–	20	0.0056
513–501	Clayey silt with sand	0.58	9	80	0.0073
501–486	Sandy gravel	0.55	24	390	0.0014
486–482	Sand with gravel	0.35	15	156	0.0022
482–475	Sand with gravel	0.60	10	234	0.0026
475–464	Gravelly sand	0.95	27	427	0.0022
464–456	Gravelly sand	0.81	41	696	0.0012
456–444	Gravelly sand	0.66	29	801	0.0008
444–432	Gravelly sand	1.11	27	565	0.0020
432–422	Gravelly sand	1.83	30	538	0.0034

Note: The unit shaft resistances were corrected for residual loads.

TABLE 6.3

Dimensions used to calculate the bearing capacity of the piles supporting pier 7

	Test Pile	Production Pile
Inner Diameter	22.00 in	22.50 in
Outer Diameter	26.00 in	24.0 in
Annulus Thickness	2.00 in	0.75 in

TABLE 6.4

LRFD design check for production piles at pier 7

Base Elevation (ft)	$Q_{sL}^n$ (kips)	$Q_b^n$ (kips)	Total Nominal Resistance (kips)	$(RF_b Q_b^n + RF_s Q_{sL}^n) \eta_g$	Total Factored Load (kips)	Pass the LRFD Check?
420	378	243	621	497	616	No
415	435	243	679	543	616	No
410	493	243	736	589	616	No
405	550	243	794	635	616	Yes

used to estimate the base resistance of the open-ended production piles. Considering that both the cone resistance  $q_c$  and the SPT blow count  $N_{SPT}$  increased with depth below the elevation of the base of the test pile (as shown in Figure 2.3), it is conservative to use the same unit annulus and plug resistances of the test pile to estimate the base resistance of the production piles, as the base of the production piles were expected to be deeper than the test pile. Alternatively, when static load test data is not available, the Purdue-INDOT pile design method (Han, Ganju, Prezzi, & Salgado, 2019; Han, Ganju, Salgado, & Prezzi, 2018, 2019) could be used to estimate the unit resistances ( $q_{sL}$ ,  $q_{ann}$ , and  $q_{plug}$ ) of the production piles. Table 6.3 summarizes the dimensions of the test and production piles that were used in the resistance calculations.

Table 6.4 shows an example of the LRFD design of the production open-ended pipe piles of pier 7. Because both the CPT cone resistance  $q_c$  and the SPT blow count  $N_{SPT}$  increase with depth below an elevation of 420 ft, indicating the presence of a strong soil layer, a pile base elevation equal to or deeper than 420 ft was considered in design. As the base elevation of the

production pile is varied, the total factored resistance  $(RF_b Q_b^n + RF_s Q_{sL}^n) \eta_g$  was calculated and compared with the total factored axial load  $LF_{DL} DL^n + LF_{LL} LL^n$ , which is equal to 616 kips for each pile of pier 7, according to the loads provided by INDOT. For a base elevation of the production pile of 405 ft, Inequality 6.1 is satisfied.

This design example above is based on the unit resistances of the test pile corresponding to the ultimate state, and thus, it is applicable for the production pile at the ultimate state, which corresponds to a pile head settlement of 10%B ( $= 10\% \times 610 \text{ mm} = 61 \text{ mm}$ ) (Han, Bisht, et al., 2019; Han, Prezzi, & Salgado, 2018; Han, Prezzi, et al., 2017; Han, Salgado, & Prezzi, 2018; Han, Salgado, et al., 2017; Jardine et al., 2005; Lehane et al., 2005; Salgado, 2008). Almost 2 years have passed since the construction of the Sagamore Parkway Bridge was completed in 2018. The monitoring of the bridge during and after construction shows that the bridge has performed well under dead and live loads, with only minimal settlement (less than 6 mm) measured, which is less than not only the ultimate limit state settlement ( $= 61 \text{ mm}$ ), but also all



the serviceability limit state settlement criteria introduced in Section 4.2. This proves the successful foundation design based on the high-quality data obtained from the static load tests.

## 7. SUMMARY AND CONCLUSION

The eastbound Sagamore Parkway Bridge was constructed from 2016 to 2018. A bridge pier (pier 7) and all of the fifteen piles supporting it were instrumented with sensors to monitor the bridge and the foundation response under dead and live loads. The pier settlement was measured using a digital level and a polymer barcode sticker attached on the bridge pier. Ten rebar (sister-bar) vibrating-wire (VW) strain gauges and five concrete-embedded VW strain gauges were installed in the pier column near the bottom of it to measure the load transferred through the bridge pier. A pair of arc-weldable VW strain gauges were installed on each of the fifteen piles under pier 7 to obtain the load distribution among the piles in the group.

The pier settlement and the dead load (resulting from the weight of the superstructure) transferred from the bridge pier to its foundation elements were monitored during the bridge construction stages. The load-settlement response of pier 7 during the bridge construction was almost linear. A total settlement of 5.2 mm was obtained for pier 7 from November 15, 2016 to March 17, 2020. The secant stiffness (slope from the origin to the point being considered) of an average pile in the 3 × 5 pile group was 46.4 kips/mm calculated at a settlement level of 5 mm; this value is about 61% of that (76.4 kips/mm) of the single, open-ended test pile, as measured in the static pile load test. At the end of bridge construction (on November 16, 2018), the piles under pier 7 carried about 77% (= 3,725 kips) of the total superstructure load (= 4,869 kips) from the pier, and the remaining 23% of the total superstructure load (1,145 kips) was carried by the pile cap. The average dead load per pile under pier 7 was measured to be 248 kips at the completion of the bridge construction. Assuming that the dead loads were carried only by the piles (no dead load carried by the soil under the pile cap), the average dead load per pile is 325 kips, which is in good agreement with the unfactored design dead load of 336 kips per pile.

A live load test was performed in seven load steps by parking twelve loaded triaxle trucks at specified locations on the bridge deck near pier 7 in a sequence that simulates a group of trucks approaching the bridge pier, parking for a period of time at specified locations, driving over the pier and leaving the bridge. Due to the locations where the trucks parked on the bridge deck, a resultant load eccentricity of 5 ft resulted. This load eccentricity was reflected in the load distribution within the bridge pier and among the fifteen piles in the group under the pier: greater loads were measured in the pier sections or piles located on the north side of the bridge. The maximum live load (in step 4) on the pier was 460 kips (2,046 kN), leading to a ratio of 16% between the

live load and the dead load on the bridge pier under the conditions considered in the present study. About 50% of the live load applied on the bridge pier was carried by the piles, and the remaining 50% was carried by the soil below the pile cap. This ratio is different from that obtained for the dead loads (about 77% of the load was carried by the piles at the end of bridge construction). The maximum vertical live load carried by a pile in the group under pier 7 was measured as 23 kips at load step 4 during the live load test. Assuming that the pile cap did not carry any load (to be consistent with the bridge design assumptions), the maximum live load carried by a pile in the group is 53 kips. This is in close agreement with the maximum unfactored live loads in a pile obtained from simulations performed of the live load test by Parsons Corporation; the maximum unfactored live loads in a pile are 62 kips and 51 kips assuming continuous-span and simple-span bridge models, respectively.

The monitoring of the bridge during and after bridge construction has shown that the bridge has performed well under dead and live loads, proving the successful foundation design based on the high-quality data obtained from the static load tests. Continuous monitoring using a wireless module is recommended to obtain load and settlement data in the long term.

## REFERENCES

- AASHTO. (2018). *AASHTO LRFD bridge design specifications*. American Association of State Highway and Transportation Officials.
- ASTM C469/C469M. (2014). *Standard test method for static modulus of elasticity and Poisson's ratio of concrete in compression*. ASTM International. <https://doi.org/10.1520/C0469>
- ASTM D2487-17. (2017). *Standard practice for classification of soils for engineering purposes (unified soil classification system)*. ASTM International. <https://doi.org/10.1520/D2487-17>
- Bozozuk, M. (1978). Bridge foundations move. *Transportation Research Record*, (678), 17–21.
- Camp, M. J., & Richardson, G. T. (1999). *Roadside geology of Indiana*. Mountain Press.
- Dasenbrock, D. D., Mattison, D. J., & Budge, A. S. (2012). Measured live load effects on driven pipe piles with established dragload. In M. L. Nuttmann (Ed.), *Proceedings of the University of Minnesota 60th Annual Geotechnical Engineering Conference*. University of Minnesota.
- Ganju, E., Han, F., Prezzi, M., & Salgado, R. (2020). Static capacity of closed-ended pipe pile driven in gravelly sand. *Journal of Geotechnical and Geoenvironmental Engineering*, 146(4), 04020008. [https://doi.org/10.1061/\(ASCE\)GT.1943-5606.0002215](https://doi.org/10.1061/(ASCE)GT.1943-5606.0002215)
- Grover, R. A. (1978). Movements of bridge abutments and settlements of approach pavements in Ohio. In: *Transportation Research Record*, (678). National Academy of Sciences.
- Han, F., Bisht, V., Prezzi, M., & Salgado, R. (2019). Validation of pile design methods for closed-ended driven pipe piles. In *Geo-Congress 2019* (pp. 98–110). American Society of Civil Engineers. <https://doi.org/10.1061/9780784482094.010>

- Han, F., Ganju, E., Prezzi, M., & Salgado, R. (2019). Closure to "Effects of interface roughness, particle geometry, and gradation on the sand-steel interface friction angle" by Fei Han, Eshan Ganju, Rodrigo Salgado, and Monica Prezzi. *Journal of Geotechnical and Geoenvironmental Engineering*, 145(11), 07019017. [https://doi.org/10.1061/\(ASCE\)GT.1943-5606.0002172](https://doi.org/10.1061/(ASCE)GT.1943-5606.0002172)
- Han, F., Ganju, E., Prezzi, M., Salgado, R., & Zaheer, M. (2020). Axial resistance of open-ended pipe pile driven in gravelly sand. *Géotechnique*, 70(2), 138–152. <https://doi.org/10.1680/jgeot.18.P.117>
- Han, F., Ganju, E., Salgado, R., & Prezzi, M. (2018). Effects of interface roughness, particle geometry, and gradation on the sand-steel interface friction angle. *Journal of Geotechnical and Geoenvironmental Engineering*, 144(12), 04018096. [https://doi.org/10.1061/\(ASCE\)GT.1943-5606.0001990](https://doi.org/10.1061/(ASCE)GT.1943-5606.0001990)
- Han, F., Ganju, E., Salgado, R., & Prezzi, M. (2019). Comparison of the load response of closed-ended and open-ended pipe piles driven in gravelly sand. *Acta Geotechnica*, 14(6), 1785–1803. <https://doi.org/10.1007/s11440-019-00863-1>
- Han, F., Ganju, E., Salgado, R., & Prezzi, M. (2020). Static load test on open-ended pipe pile using double-wall instrumentation. In *Geo-Congress 2020* (pp. 73–81). American Society of Civil Engineers. <https://doi.org/10.1061/9780784482780.008>
- Han, F., Ganju, E., Salgado, R., Prezzi, M., & Zaheer, M. (2019). *Experimental study of the load response of large diameter closed-ended and open-ended pipe piles installed in alluvial soil*. (Joint Transportation Research Program Publication No. FHWA/IN/JTRP-2019/03). West Lafayette, IN: Purdue University. <https://doi.org/10.5703/1288284316880>
- Han, F., Lim, J., Salgado, R., Prezzi, M., & Zaheer, M. (2015). *Load and resistance factor design of bridge foundations accounting for pile group-soil interaction* (Joint Transportation Research Program Publication No. FHWA/IN/JTRP-2015/24). West Lafayette, IN: Purdue University. <https://doi.org/10.5703/1288284316009>
- Han, F., Marashi, M., Prezzi, M., Salgado, R., Wells, T., & Zaheer, M. (2020, December 15). Live load test on the Sagamore Parkway Bridge over the Wabash River. *Transportation Research Record*. <https://doi.org/10.1177/0361198120971263>
- Han, F., Prezzi, M., & Salgado, R. (2018). Static and dynamic pile load tests on closed-ended driven pipe pile. In *International Foundations Congress and Equipment Exposition (IFCEE 2018)* (pp. 496–506). American Society of Civil Engineers. <https://doi.org/10.1061/9780784481578.047>
- Han, F., Prezzi, M., Salgado, R., & Zaheer, M. (2017, March). Axial resistance of closed-ended steel-pipe piles driven in multilayered soil. *Journal of Geotechnical and Geoenvironmental Engineering*, 143(3), 04016102. [https://doi.org/10.1061/\(ASCE\)GT.1943-5606.0001589](https://doi.org/10.1061/(ASCE)GT.1943-5606.0001589)
- Han, F., Salgado, R., & Prezzi, M. (2018). Numerical and experimental study of axially loaded non-displacement piles in sand. In *Proceeding of the 2018 International Conference on Deep Foundations and Ground Improvement* (pp. 221–229). Deep Foundations Institute.
- Han, F., Salgado, R., Prezzi, M., & Lim, J. (2017, March). Shaft and base resistance of non-displacement piles in sand. *Computers and Geotechnics*, 83, 184–197. <https://doi.org/10.1016/j.compgeo.2016.11.006>
- Han, F., Salgado, R., Prezzi, M., & Lim, J. (2019, July). Axial resistance of nondisplacement pile groups in sand. *Journal of Geotechnical and Geoenvironmental Engineering*, 145(7), 04019027. [https://doi.org/10.1061/\(ASCE\)GT.1943-5606.0002050](https://doi.org/10.1061/(ASCE)GT.1943-5606.0002050)
- Hill, J. R. (2019). *Landscapes of Indiana*. Indiana Geological & Water Survey. <https://igws.indiana.edu/Surficial/Landscapes>
- INDOT. (2013). *Indiana design manual-2013* [Webpage]. Indiana Department of Transportation. <https://www.in.gov/dot/div/contracts/design/IDM.htm>
- Jardine, R., Chow, F., Overy, R., Standing, J., & Jamie, S. (2005). *ICP design methods for driven piles in sands and clays*. Thomas Telford Ltd. <https://doi.org/10.1680/idmfd.pisac.32729>
- Kolk, H. J., Baaijens, A. E., & Senders, M. (2005). Design criteria for pipe piles in silica sands. In *Proceedings of the 1st International Symposium on Frontiers in Offshore Geotechnics* (pp. 711–716). Taylor & Francis. <http://www.scopus.com/inward/record.url?eid=2-s2.0-84857486645&partnerID=tZOtx3y1>
- Lehane, B., Schneider, J., & Xu, X. (2005). The UWA-05 method for prediction of axial capacity of driven piles in sand. In M. J. Cassidy, & S. Gourvenec. (Eds.), *Proceedings of the International Symposium on Frontiers in Offshore Geotechnics (IS-FOG 2005)* (pp. 683–689). CRC Press/Balkema.
- Mandolini, A., Russo, G., & Viggiani, C. (2005). Pile foundations: Experimental investigations, analysis and design. In *Proceedings of the 16th International Conference on Soil Mechanics and Geotechnical Engineering* (pp. 177–213). <https://doi.org/10.3233/978-1-61499-656-9-177>
- Parsons. (2016). *Bridge plans for spans over 20 Feet, E.B. US 52 over Wabash River & North River Road* (Project No. 0400774). Indiana Department of Transportation.
- Salgado, R. (2008). *The engineering of foundations*. McGraw-Hills.
- Salgado, R., Han, F., & Prezzi, M. (2017). Axial resistance of non-displacement piles and pile groups in sand. *Rivista Italiana Di Geotecnica*, 51(4), 35–46. <https://doi.org/10.19199/2017.4.0557-1405.35>
- Shulyat'ev, O. A., & Kharichkin, A. I. (2009). In-situ measurements of pile-to-pile load distribution in foundations. *Soil Mechanics and Foundation Engineering*, 46(6), 239–246. <https://doi.org/10.1007/s11204-010-9074-8>
- TOPCON. (2011). *Instruction manual: Electronic digital level DL-102C*. [http://www.toping.ro/pdf/DL-102C\(Grade%20Circle\).pdf](http://www.toping.ro/pdf/DL-102C(Grade%20Circle).pdf)
- Walkinshaw, J. L. (1978). Survey of bridge movements in the western United States. In *Transportation Research Record*, 678, 6–10. National Academy of Sciences. <https://trid.trb.org/view/91787>
- West, T. R. (2000, February 1). [Review of the *Roadside Geology of Indiana*, by Mark J. Camp and Graham T. Richardson]. *Environmental & Engineering Geosciences*, 6(1), 90–91.
- Yamashita, K., Yamada, T., & Hamada, J. (2011). Investigation of settlement and load sharing on piled rafts by monitoring full-scale structures. *Soils and Foundations*, 51(3), 513–532. <https://doi.org/10.3208/sandf.51.513>

## About the Joint Transportation Research Program (JTRP)

On March 11, 1937, the Indiana Legislature passed an act which authorized the Indiana State Highway Commission to cooperate with and assist Purdue University in developing the best methods of improving and maintaining the highways of the state and the respective counties thereof. That collaborative effort was called the Joint Highway Research Project (JHRP). In 1997 the collaborative venture was renamed as the Joint Transportation Research Program (JTRP) to reflect the state and national efforts to integrate the management and operation of various transportation modes.

The first studies of JHRP were concerned with Test Road No. 1 — evaluation of the weathering characteristics of stabilized materials. After World War II, the JHRP program grew substantially and was regularly producing technical reports. Over 1,600 technical reports are now available, published as part of the JHRP and subsequently JTRP collaborative venture between Purdue University and what is now the Indiana Department of Transportation.

Free online access to all reports is provided through a unique collaboration between JTRP and Purdue Libraries. These are available at <http://docs.lib.purdue.edu/jtrp>.

Further information about JTRP and its current research program is available at <http://www.purdue.edu/jtrp>.

## About This Report

An open access version of this publication is available online. See the URL in the citation below.

Han, F., Prezzi, M., Salgado, R., Marashi, M., Wells, T., & Zaheer, M. (2020). *Verification of bridge foundation design assumptions and calculations* (Joint Transportation Research Program Publication No. FHWA/IN/JTRP-2020/18). West Lafayette, IN: Purdue University. <https://doi.org/10.5703/1288284317084>